Developing a supported metal oxide catalyst for direct dehydrogenation of propane to propene

Rajvikram Singh, Raghvendra Singh, Goutam Deo

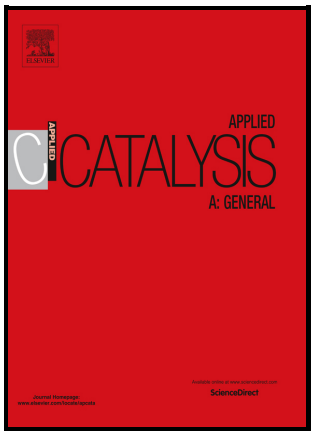

PII: S0926-860X(25)00255-8

DOI: https://doi.org/10.1016/j.apcata.2025.120354

Reference: APCATA120354

To appear in: *Applied Catalysis A, General*

Received date: 12 March 2025
Revised date: 10 May 2025
Accepted date: 18 May 2025

Please cite this article as: Rajvikram Singh, Raghvendra Singh and Goutam Deo, Developing a supported metal oxide catalyst for direct dehydrogenation of propane to propene, *Applied Catalysis A, General,* (2025) doi:https://doi.org/10.1016/j.apcata.2025.120354

Developing a supported metal oxide catalyst for direct dehydrogenation of propane to propene

Rajvikram Singh, Raghvendra Singh and Goutam Deo*

Department of Chemical Engineering

Indian Institute of Technology Kanpur

Kanpur, 208016, INDIA

*** Corresponding author: goutam@iitk.ac.in**

Abstract

Propene is an important building block in the petrochemical industry and its demand is rapidly increasing. However, the production through conventional processes is limited, and there is a dire need to develop a suitable catalyst for the direct dehydrogenation of propane. Multiple set of catalysts are synthesized via incipient wetness impregnation method and characterized by various techniques. These catalysts are also tested for the direct dehydrogenation reaction, to examine the effect of active metal oxide species, support material, metal oxide loading and potassium (K) loading. Subsequently, the reaction temperature and contact time are optimized for the reaction. A near-monolayer loading chromium oxide supported on ZrO_2 is the most active. At this loading incipient amounts of Cr_2O_3 crystallites are detected, which became larger at higher coverages. The monolayer coverage appears to be between 5.2 to 6.6 $atom_{Cr}/nm^2$. Furthermore, at this coverage the amount of reducible Cr^{+6} species was maximum. The activity of this near-monolayer catalyst is further improved by co-impregnating K. A Cr to K molar ratio of 1:0.05 is found to increase the amount of reducible Cr^{+6} and the catalyst activity and selectivity. Increasing the K amount further leads to a decrease in activity. Activity is increased by increasing the reaction temperature till 550 °C; however, above 550 °C the catalyst deactivates due to coke formation. Further improvement in activity is achieved by increasing

the contact time and a conversion of ~30% and yield of ~27% is achieved for the K-promoted supported chromia catalyst at 550°C and a contact time of 37.33 $g_{cat}.h/mol$.

Keywords

Propane, Propene, $CrZrO_2$ catalysts, potassium promotion, Reaction temperature, Contact time

1. Introduction

Propene (C_3H_6) continues to hold a significant role being one of the foundational precursors in the petrochemical industry, boasting a multitude of applications. These applications include the production of polypropylene, cumene, acrylonitrile, isopropyl alcohol, and several others [1-3]**.** In the last two decades, the demand for C_3H_6 has increased substantially. It is projected to experience further growth over the following decades. In 2019, the yearly production of C_3H_6 was approximately 130 million metric tonnes (MMT), and projections indicate that the production will rise to 191 MMT by the year 2030 [4].

Recent trends indicate that production through traditional methods, particularly steam reforming and fluid catalytic cracking, is not increasing at the same rate as the growing demand [5]. This disparity in rates can be attributed to the fact that C_3H_6 is not the primary product of these conventional processes. Attempts have also been made to produce large-scale C_3H_6 via extraction of propane from shale gas [6,7]. However, this method also involves cracking as part of the overall process which leads to challenges related to the energy-intensive nature of the process and catalyst deactivation [8]. Consequently, there is a need to develop alternate processes to reduce the "supply-demand gap".

Propane Dehydrogenation (PDH) is among the processes which produces C_3H_6 and has been implemented at an industrial scale [9]. Commercial PDH processes rely exclusively on catalysts derived from either Pt or Cr as the main component [5,10]. Furthermore, these

catalysts are primarily supported on an Al_2O_3 support and use different types of promoters [9,11]. However, the PDH reaction does pose certain hurdles, which need to be overcome. The PDH is an endothermic reaction, requiring elevated temperatures to obtain reasonable conversions [5]**.** Unfortunately, it appears that with an increase in operating temperature, the formation of coke also rises, and catalyst deactivation occurs [5]. Thus, to overcome the disadvantages of the PDH process mentioned above, a suitable catalyst is required.

For the PDH reaction, an exhaustive list of catalysts has been tested, as mentioned in recent reviews [5,9,12–14]. These include several supported metal-based and metal oxide-based catalysts. In supported metal oxide catalysts, which is the focus of the current study, there exists an active metal oxide phase, supported on a high surface area oxide [15–17]. Furthermore, the commonly used surface metal oxide phase for the PDH reaction is based on chromium oxide (chromia). Since the pioneering efforts by Frey and Huppke [18]**,** chromia catalysts have been extensively investigated. Alumina-supported chromia, with an alkali promoter, is used as an industrial catalyst for the CATOFIN process [19]. Several other supported metal oxides have also been tried for the PDH reaction. These include the oxides of vanadium, gallium, zinc, iron, copper, indium, and molybdenum [20–27]**.**

The support also plays a significant contribution in supported metal oxide catalysts for the PDH reaction. There have been several metal oxides and mixtures of metal oxides used as supports. Some of them are: CeO_2, Al_2O_3, SiO_2, TiO_2, ZrO_2, CeO_2-ZrO_2, Nb_2O_5, TiO_2-Al_2O_3 and CeO_2-Al_2O_3 [21,28–42]. Though the industrial catalyst is based on an Al_2O_3 support, a few studies show that the ZrO_2 supported chromia catalyst provides a higher turnover frequency [43–45]. This opens several opportunities to enhance the existing activity of the supported chromia catalyst.

In addition to the choice of the active metal oxide and the support material, the activity of the catalyst for the PDH reaction can be enhanced by using a suitable promoter. The promoters

used are often alkali metals, namely Li, Na, K and Cs [46–51]. Out of these K is the commonly used promoter, that is also used in the commercial catalyst.

In addition to the three factors mentioned above in the context of supported metal-oxide catalysts, namely, active metal-oxide phase, specific oxide support, and promoters, other factors do play an important role. Proper synthesis of the supported metal oxide catalyst is critical since the active phase must be present on the surface of the oxide support. There are several methods to prepare catalyst samples [52], but incipient wetness impregnation (IWI) is one of the most commonly used methods to synthesize supported metal oxide catalysts due to its simplicity for lab-scale synthesis. Furthermore, the amounts of active metal oxide phase and promoter are important so that the conversion of propane during the PDH process is maximized [43,49,53]**.**

During the development of a suitable supported metal-oxide catalyst, various characterization methods have been employed to ensure the proper synthesis of the catalyst and to facilitate the understanding of the effect of different factors [35,50,54]. One of the main aims of the characterization techniques for supported metal oxide catalysts is to confirm the presence of the surface metal oxide phase and establish monolayer loadings. Establishing the monolayer coverage provides the limit for the development of surface bound metal-oxide species since above monolayer coverage crystallite or bulk surface metal oxide species exist [55,56]. Several previous assessments have demonstrated that the surface metal-oxide phase at or below the monolayer is more active than the crystalline or bulk metal oxide species [57–59]**.** The monolayer loadings of a few surface metal oxide phases on different oxide supports have been tabulated previously [17,60,61]**.** Furthermore, characterization of the spent catalyst provides important information about the possible changes that the catalysts might have undergone.

Due to the interplay amongst the various factors, it is challenging to formulate a suitable catalyst. In this study, we proceed systematically toward optimizing four factors for the PDH

reaction. These factors are: (i) the active metal oxide phase, (ii) the oxide support used to support the most active metal oxide phase, (iii) the loading of most active metal-oxide phase, and (iv) the use of different loadings of a promoter to try to enhance the catalytic activity further. de Rossi et al. also followed a similar strategy for developing a catalyst for the PDH reaction; however, the first factor was not considered [49]. Furthermore, in their study they did not observe promotion with potassium addition, which we found surprising. We intend to examine this absence of promotion in more detail. While formulating a suitable catalyst we limit our study to using the incipient wetness impregnation method for catalyst synthesis and carrying out the PDH reaction at 550°C and a lower partial pressure of propane. The choice of a reaction temperature of 550°C is common to several studies available on the PDH reaction [5,23,59,62–64]. Low partial pressures of propane and appropriate contact times are chosen to distinguish the catalysts based on the kinetics of the reaction as done previously [59,63,65,66]. The catalysts are analysed for their surface area, and by UV-vis spectroscopy, Raman spectroscopy, and temperature programmed reduction using H_2 (H_2-TPR). A few catalysts (fresh and spent) are also characterized by X-ray photoelectron spectroscopy (XPS). We restrict our choice of surface metal oxide phase to transitional metal oxides of chromium, vanadium, and iron, and the metal oxide support to Al_2O_3, CeO_2, Nb_2O_5, TiO_2 and ZrO_2. Furthermore, the surface metal oxide amounts range from less than monolayer loadings to above monolayer loadings, and the potassium to chromium molar ratio ranges from 0.05 to 0.20. By proceeding in a stepwise manner, we expect to develop the best performing catalyst, and for this catalyst we studied the effect of reaction temperature and contact time to obtain the highest achievable conversions of propane. Thus, we expect to develop the most suitable supported metal oxide catalyst, from the limited scope of transitional metal oxides and oxide supports, for the PDH reaction.

2. Experimental Procedures

2.1 Catalyst synthesis

Four sets of catalysts were prepared using the incipient-wetness-impregnation method to investigate the effects of the four chosen variables that affect the performance of the catalyst. Additional details about the incipient-wetness-impregnation method are given in the supplementary information file. The four sets of catalysts are:

1. The first set of catalysts was prepared to examine the effect of the oxides of chromium, vanadium and iron. The precursors used to synthesize these supported transitional metal oxides were: (i) chromium nitrate ($Cr(NO_3)_3.9H_2O$, Fluka) for chromium oxide, (ii) ammonium metavandate (NH_4VO_3, LOBA Chemie) and oxalic acid ($(COOH)_2.2H_2O$, Fisher Scientific) for vanadium oxide, and (iii) iron nitrate ($Fe(NO_3)_3.9H_2O$, SDFCL) for iron oxide. The support selected for this set of catalysts was ZrO_2 (Saint Gobain). Equal metal loading (2wt. %) was chosen. This metal loading was chosen so that they were less than monolayer amounts [67–69].

2. Based on the best supported transition metal oxide determined above second set of catalysts was used to study the effect of the oxide support. The supports shortlisted were: Al_2O_3, CeO_2, Nb_2O_5, TiO_2 and ZrO_2. Here again the transition metal loading (2 wt.%) was less than monolayer amounts [17,37]. Certain details of the supports are mentioned in Table S1 of the supporting information file.

3. After choosing the active metal-oxide and the oxide support, the third set of catalysts were used to analyse the effect of active metal-oxide loading. To analyse this effect, the metal-oxide loading was varied to achieve sub-monolayer to above monolayer coverages.

4. To enhance the catalytic activity of the best performing supported metal-oxide catalyst determined above, the fourth and last set of catalysts were employed to investigate the effect of a promoter and promoter amount. Potassium (K) was chosen as a promoter, and the corresponding precursor was potassium nitrate (KNO_3, Sigma).

The details of all the prepared catalysts, such as its nomenclature, amount of metal and promoter in the catalysts are given in Table S2 of the supporting information file. The nomenclature was based on the loading of metal-oxide, type of the metal-oxide, loading of potassium (promoter) and support used. For example, a nomenclature of xMS referred to x% of transition metal M in the catalyst containing a support S, where M = Cr, V or Fe and S = Al (for Al_2O_3), Ce (for CeO_2), Nb (for Nb_2O_5), Ti (for TiO_2) and Zr (for ZrO_2). For potassium containing catalysts, the nomenclature was 2.5CryK, where the chromium loading was 2.5% and the molar ratio of K to Cr was 'y', and the support used was ZrO_2, which is not mentioned in the nomenclature of these potassium containing supported chromia catalysts.

2.2 Catalyst characterization

2.2.1 Elemental composition and surface area measurement

The elemental composition of the prepared samples was measured to confirm its closeness to the nominal values by EDX scans conducted using a Supra 40VP scanning electron microscope (Zeiss, Germany) operated at an accelerating voltage of 10 kV. To prevent surface charging during imaging, the samples were coated with a thin layer of gold.

The specific surface area of the synthesized catalysts and supports were measured using multi-point BET equation. To determine the surface area, N_2 adsorption data at -196^{o}C was obtained using an Autosorb iQ TPX equipment (Quantachrome, USA). Nearly 200 mg sample was degassed at 150°C for 6 h before N_2 adsorption.

2.2.2 H_2-TPR studies

The H_2-TPR studies were performed for all the synthesized catalysts and supports by loading an amount of 60 mg sample in the sample-cell of an AMI 200 (Altamira, USA) set-up. It used a thermal conductivity detector (TCD) for determining the effluent composition, which measured the H_2-uptake (mol/g_{cat}). The detailed procedure about running the TPR and obtaining the H_2-uptake, T_{max} from H_2-TPR profile has been described previously [70].

2.2.3 UV-vis spectroscopy

The UV-vis spectra of all the catalysts and supports were collected using a UV-vis-NIR 5000 (Varian, USA) spectrometer. All samples were scanned in the range of 200-800 nm under atmospheric conditions. $BaSO_4$ (barium sulphate, Sigma Aldrich) was used as reference, unless mentioned otherwise.

2.2.4 Raman spectroscopy

All the prepared supports, catalysts and some of the spent catalyst samples were scanned using an Acton Spectra Pro 2500i (Princeton Instrument, USA) instrument to obtain the Raman spectra. The instrument utilized a 532 nm diode-pumped solid-state laser for all the scans, it was running at 50% strength with a maximum power of 40mW. The magnification was achieved using 20X and 50X objective lenses. The spectra were recorded under ambient temperature and pressure acquiring 20 successive scans, each with an acquisition time of 2 s.

2.2.5 X-ray photoelectron spectroscopy

The XPS spectra of representative fresh catalysts were collected using a NEXSA (Theroscientific, USA) instrument. The X-ray source employed was Al Kα monochromatic laser. The spectra were recorded under ultra-high vacuum conditions, maintaining a base pressure of $3*10^{-9}$ mbar. The acquired spectra were calibrated using the adventitious carbon peak at 284.8 eV as the reference to avoid charging error [70–72].

2.3 Reactivity studies

The reactivity parameters of the PDH reaction were determined for the catalysts using a down-flow quartz–tube packed bed reactor operating under ambient pressure. A thermocouple was positioned above the catalyst bed to monitor the bed temperature. Pre-reaction, each catalyst sample was activated by in-situ calcination in an O_2 atmosphere (1.80 $L.h^{-1}$ flow) at 550°C for 1 h. Post-calcination, all traces of O_2 was removed from the reactor by purging with N_2, flowing at 1.80 $L.h^{-1}$ for 0.5 h. The PDH reaction was performed at 550^oC using a C_3H_8-N_2 mixture

flowing through the reactor at 1.80 L.h^{-1}, with a partial pressure of C_3H_8 = 0.075 atm. The O_2-ODH reactions were performed at the same temperature and atmospheric pressure. The reactant mixture of C_3H_8 and O_2 was fed in stoichiometric ratio (2:1). The partial pressure of propane was kept at 0.075 atm and N_2 was used as an inert. Each reaction was repeated at least three times, and the average value was reported. The standard deviation of the repeat experiments was considered as the error, which was also reported. At the exit of the reactor, the effluent gas was mixed with a 0.12 L.h^{-1} CH_4 stream. The CH_4 stream acted as an external standard and was used for calculation purposes. All volumetric flowrates were maintained using separate mass flow controllers (Bronkhorst), which were usually in the range of 0-50 mL/min and a standard error of 1% of full scale. Afterwards, the gas mixture was directed through the condenser to eliminate moisture remnants. At different time-on-stream (TOS) the condenser effluent was collected, and molar composition was analysed with a Nucon 5765 gas chromatograph (GC) (Nucon, India)). The GC was equipped with a TCD and flame ionization detector (FID). A Carbosphere column was attached to the TCD and a HySepQ column was attached to the FID. The peak area of each component was recorded, and it was used to compute the conversions and yields. The response factors of the gaseous components were calculated by either using pure gas mixtures or a standard gas mixture (Chemtron Science Laboratories Pvt. Ltd.) containing known mol fractions of relevant gases. The conversion of C_3H_8 ($X_{C_3H_8}$) and yield of C_3H_6 ($Y_{C_3H_6}$) was calculated by equation (1) and (2), respectively. The corresponding turnover frequencies (TOF) were also calculated by equation (3) and (4).

$$X_{C_3H_8}(\%) = \left(1 - \frac{\frac{F_{C_3H_8\ OUT}}{F_{CH_4\ OUT}}}{\frac{F_{C_3H_8\ IN}}{F_{CH_4\ IN}}}\right) * 100 \qquad (1)$$

$$Y_{C_3H_6}(\%) = \left(\frac{\frac{F_{C_3H_6\ OUT}}{F_{CH_4\ OUT}}}{\frac{F_{C_3H_8\ IN}}{F_{CH_4\ IN}}} \right) * 100 \quad (2)$$

$$TOF_{C_3H_6} = \left(\frac{F_{C_3H_6,out}}{W * H_2 - uptake} \right) (s^{-1}) \quad (3)$$

$$TOF_{C_3H_8} = \left(\frac{F_{C_3H_8,in} - F_{C_3H_8,out}}{W * H_2 - uptake} \right) (s^{-1}) \quad (4)$$

In equations (1) to (4), F_i is the molar flow rate of the species i, W is the mass of the catalyst, and $H_2 - uptake$ is the mol of H_2 per gram of the catalyst. The carbon balance, $\frac{mol\ C_{out}}{mol\ C_{in}} * 100$, was determined for each run and was found to be better than 98%.

3. Result and Discussion

Four sets of catalysts were prepared and tested by various characterisation techniques. Subsequently, the catalysts were evaluated for the PDH reaction. The results based on these studies are presented and discussed below.

3.1. Elemental composition and surface area studies

The actual amount of metal and promoter amount was determined from EDX analysis, is shown in Table S3 of the supplementary information file. The EDX count data for all the samples are shown in Figure S1 of the supplementary information file. The EDX data shows close similarity between nominal and actual amount of metal/promoter.

The surface areas of most samples were determined and listed along with the surface areas of the pre-treated supports in Table S1 and Tables S4 to S7. Relevant information from H_2-TPR studies is also included in these tables and are discussed later. A slight change in surface area was observed as the metal loading increased on a specific support. For example, the surface area of ZrO_2 support is 48 m^2/g. and all the supported catalysts using ZrO_2 as the support are

between 42 and 45 m^2/g with no specific trend. Such small changes in surface area have also been shown by others [37,67,72,73].

3.2. UV-vis spectroscopy studies

The UV-vis spectra of each set of the prepared samples were recorded under standard conditions in the 200 nm to 800 nm region. The UV-Vis spectra of the supports (Al_2O_3, CeO_2, Nb_2O_5, TiO_2, and ZrO_2) are shown in Figure S2 of the supporting information file and discussed there. The UV spectra of 2MZr, where M = Cr, V or Fe, are presented in Figure S3 of the supplementary information file. In these spectra the support was used as the reference so that the electronic transitions due to the oxides of Cr, V and Fe are clearly seen. For 2CrZr, we see two major bands at 278 nm and 359 nm, which correspond to the Cr^{+6} oxidation state [37,74] and for 2VZr we see a broad peak at ~350 nm, which corresponds to the V^{+5} oxidation state [75]. For 2FeZr, a band at ~350 nm reveals the presence of Fe^{+3} [76,77] and a band at ~540 nm is characteristic band of ά-Fe_2O_3 [72,77–80].

The UV-vis spectra of the 2CrS catalysts, where S = Al_2O_3, CeO_2, Nb_2O_5, TiO_2 and ZrO_2, were obtained and only the spectra for 2CrZr and 2CrAl are shown in Figure S4 of the supplementary information file. In these spectra ZrO_2 and Al_2O_3 were used as the reference. The spectra of the remaining 2CrS samples were dominated by the support features and are not shown for brevity. For 2CrZr and 2CrAl two major bands corresponding to Cr^{+6} species are evident [37,74,75,81-83].

The UV spectra of the third set of catalysts, where the effect of metal loading of Cr over ZrO_2 is analysed, is shown in Figure 1. These spectra were also obtained using the ZrO_2 support as the reference. Two peaks at ~278 nm and ~370 nm, due to Cr^{+6}, are clearly seen [49,84]. The peak at ~370 nm shifts at lower wavenumber as the metal loading increases. A small band at

~600 nm is also present in 2.5CrZr and is clearly visible in the 3CrZr sample. Such a band is associated with the presence of Cr^{+3} oxide [49].

The UV-vis spectra of the last set of catalysts, which was prepared to test the effect of promoter, are shown in Figure S5 of the supplementary information file. There is no significant change in the spectra due to the presence of distinct amounts of potassium in the 2.5CryK catalysts, suggesting the continued presence of Cr^{+6} species.

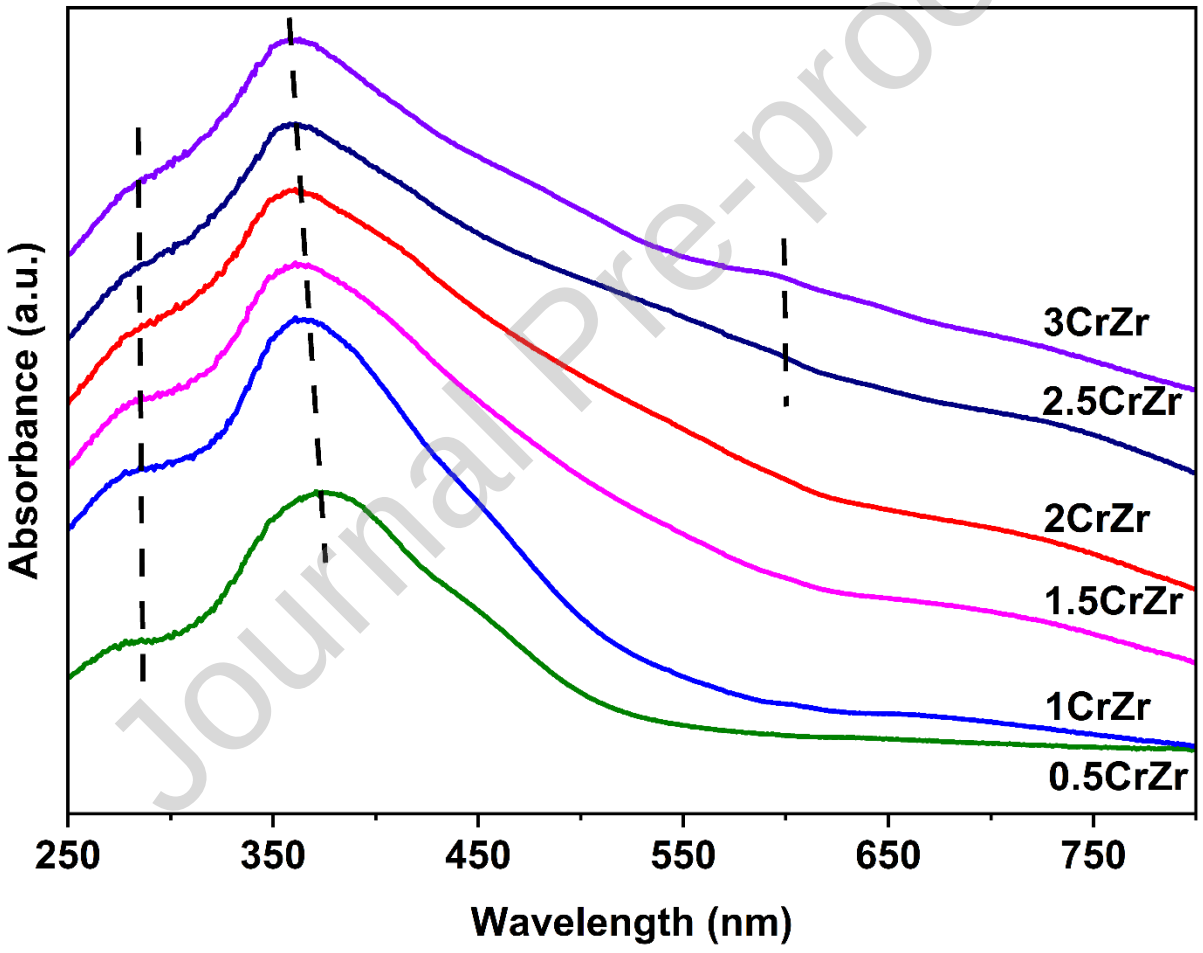

Figure 1: UV-vis spectra of xCrZr catalysts showing the effect of chromium loading, x = 0.5, 1.0, 1.5, 2.0, 2.5 and 3.0.

3.3. Raman spectroscopy studies

The four sets of supported metal oxide samples and the supports were characterised using Raman spectroscopy. The Raman spectra of the support materials (Al_2O_3, CeO_2, Nb_2O_5, TiO_2, and ZrO_2) are shown in Figure S6 of the supporting information file and discussed there. The spectra of the 2MZr samples (M = Cr, Fe or V) are shown in Figure S7 of the supplementary information file. All the spectra in Figure S7 show sharp bands due to ZrO_2 at 476, 615 and 635 cm^{-1} [85,86]. Furthermore, two broad peaks at 870 and 1035 cm^{-1} for the 2CrZr sample are seen, which corresponds to molecularly dispersed chromia species [87]. The Raman spectra of 2VZr, shows a broad band between 870-1000 cm^{-1}, due to the molecularly dispersed vanadia species [69], and the spectrum of 2FeZr only shows the Raman vibration of ZrO_2 and the bands due to iron oxide are not evident.

The Raman spectra of 2CrS, where S = Al_2O_3, CeO_2, Nb_2O_5, TiO_2 and ZrO_2, are shown in Figure S8 of the supplementary information file. In none of the spectra is a band at ~550 cm^{-1} observed, which indicates crystalline Cr_2O_3 is absent. It appears that the chromia loading for all the 2CrS samples are below monolayer coverages, which is consistent to those expected based on the surface area of the supports. As discussed above the 2CrZr sample shows the presence of molecularly dispersed surface chromia species in addition to the bands of the ZrO_2 support. For the 2CrAl, 2CrCe and 2CrTi samples, small Raman features due to molecularly dispersed chromia species are seen once the support vibrations are subtracted. For 2CrNb, the spectrum is dominated by the band of Nb_2O_5 and the presence of molecularly dispersed chromia is not evident.

The Raman spectra of xCrZr, where x = 0, 0.5, 1, 1.5, 2, 2.5 and 3 are shown in Figure 2 in the 400 to 1200 cm^{-1} region. The major peaks due to the surface chromia species are detected at ~860 cm^{-1} and ~1035 cm^{-1}. These bands correspond to the molecularly dispersed chromia species in the Cr^{+6} oxidation state [88]. As the amount of chromium increases above 2%, a band appear at 551 cm^{-1} due to the presence of Cr_2O_3 crystals [37,67,89], indicating that

monolayer coverage has been surpassed for 2.5% metal loading. Thus, the monolayer concentration of chromium species on this ZrO_2 support falls in the range of 5.2 to 6.6 $atom_{Cr}/nm^2$, which is consistent with monolayer coverage value of ~5.4 $atom_{Cr}/nm^2$ determined by previous studies [37,67,70].

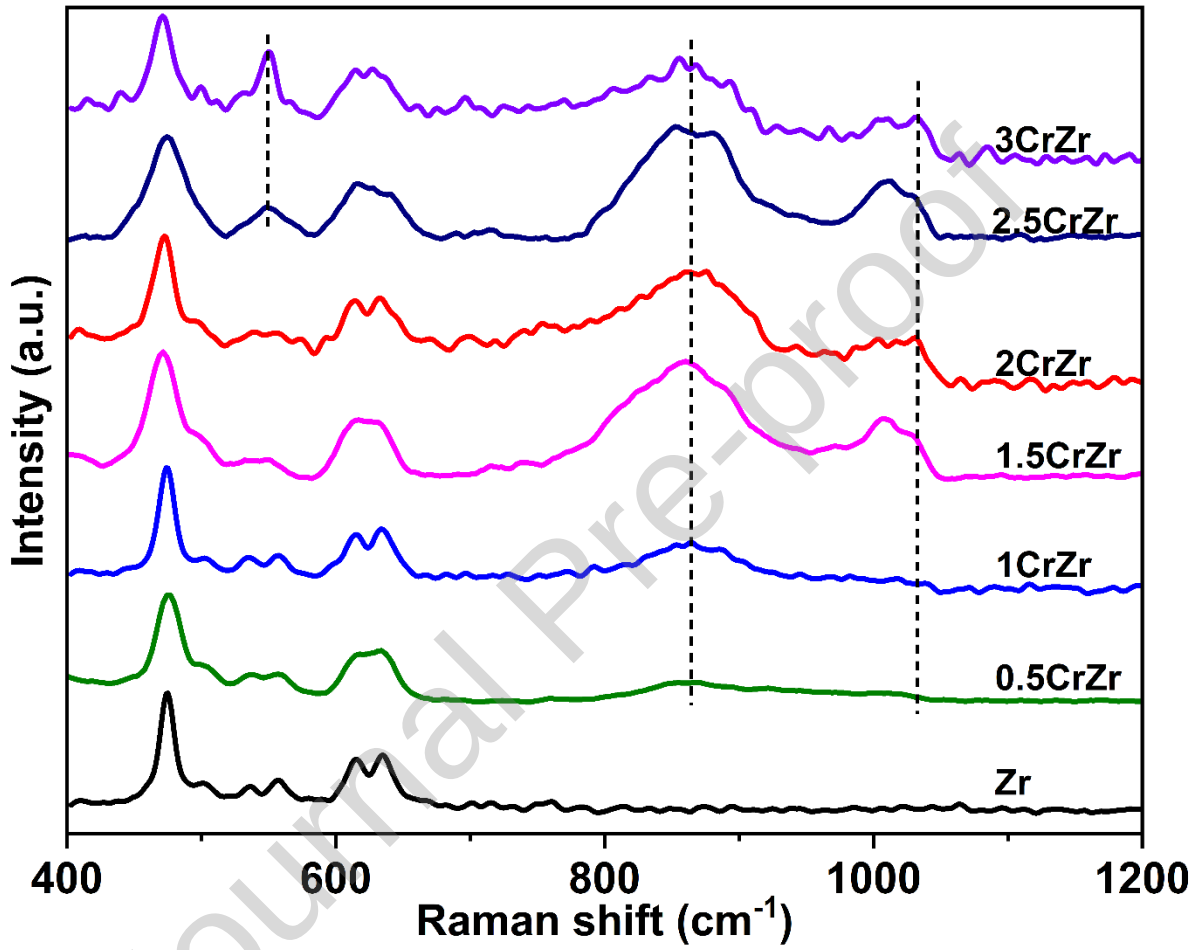

Figure 2: Raman spectra of xCrZr catalysts showing the effect of chromia loading, x = 0.5, 1.0, 1.5, 2.0, 2.5 and 3.0.

The Raman spectra of the last set of catalysts showing the effect of potassium loading are shown in Figure S9 of the supplementary information file. When the K/Cr ratio was 0.05, as in the 2.5Cr0.05K catalyst, the band at 551 cm^{-1} appears to have decreased in intensity. Furthermore, the band at ~860 cm^{-1} increased in intensity and a new band is seen at about 972 cm^{-1}. As the amount of potassium increased, two distinct bands at ~860 cm^{-1} and ~1010 cm^{-1}

were evident and a small band at ~540 cm^{-1} appeared to grow. It appears that this band is due to Cr_2O_3 [90,91]. A previous study on the XRD, UV-vis and Raman spectra of K-containing chromia/alumina samples suggested that $K_2Cr_2O_7$ is initially formed which upon heating decomposes to K_2CrO_4 and α-Cr_2O_3 [88,91]**.**

3.4. H_2 TPR studies

All the support and synthesized catalysts were characterised by H_2 TPR. From the H_2-TPR profiles obtained the reducibility of the catalysts were analysed and the $H_2 - uptake$ was determined. The temperature at which the TCD signal is maximum, T_{max}, of all the catalysts are shown on the TPR profile of the samples. The H_2 TPR profile of the support material are shown in Figure S10 of the supplementary information file. None of the supports show reduction between 200 and 600°C, except for CeO_2. The CeO_2 support shows a broad reduction peak between 300 to 550°C, with a T_{max} at 515°C.

The H_2-TPR profiles of the first set of catalyst are shown in Figure S11 and the relevant data is provided in Table S4 of the supplementary information file. The 2CrZr and 2VZr samples shows a single T_{max} which corresponds to a single reduction step [37,92]. In case of 2FeZr, two broad reduction peaks, between 200 to 600°C, were detected. These two reduction peaks are due to multiple reduction steps [93]. Furthermore, the $H_2 - uptake$ for each sample was determined and then the H/M ratio (M = Cr, V or Fe) was calculated and given in Table S4. Clearly, the H/Cr ratio is less than 3, which would have been expected for a change in oxidation state from Cr^{+6} to Cr^{+3}. Such is not the case for H/V, since a value of 2.1 closely corresponds to the reduction of V^{+5} to V^{+3}. For 2FeZr, the H/Fe ratio of 2.4 reflects the mixture of Fe^{+2} and Fe^{+3} species present in the calcined sample. A mixture of Fe^{+2} and Fe^{+3} have also been seen before in calcined ZrO_2 supported Fe-oxide catalysts [93].

The H_2-TPR profiles of the second set of catalysts, 2CrS, are shown in Figure S12. All the catalysts show a single T_{max}, which corresponds to a single step reduction process, except for

2CrCe, which shows a distinct shoulder due to the reduction of the CeO_2 support. The 2CrZr sample has the lowest T_{max} (298 °C) and 2CrAl the highest (360 °C). Previous studies also reveal that the specific support has an effect on T_{max} for supported metal oxides [37,92]. The trend in T_{max} for the 2Cr/S samples was:

$$2CrAl > 2CrCe > 2CrNb > 2CrTi > 2CrZr.$$

The $H_2 - uptake$ and H/Cr molar ratio also depend on the specific support used to make the supported metal catalyst, as shown in Table S5. The $H_2 - uptake$ and H/Cr molar ratio reveal the following trend:

$$2CrZr > 2CrAl > 2CrCe > 2CrNb > 2CrTi$$

The next set of catalysts was used to examine the effect of loading of the CrZr samples by H_2-TPR. Figure 3 reveals that as the metal loading increases, T_{max} gradually decreases, as shown by the dotted line joining the peak maxima. Such a decrease in T_{max} suggests that oxygen is less strongly bound to the supported metal oxide sample. However, the $H_2 - uptake$ increases with an increase in metal loading, as shown in Table S6. An increase in H_2-uptake is due to the additional availability of reducible surface chromia species [70]. However, the H/Cr molar ratio decreases with an increase in metal loading. A decrease in H/Cr molar ratio with loading suggest that a larger fraction of the chromia species is not reducible as the loading is increased. Such a decrease in H/Cr ratio with loading has been observed previously for chromia supported Al_2O_3, SiO_2 and TiO_2 catalysts [37,94].

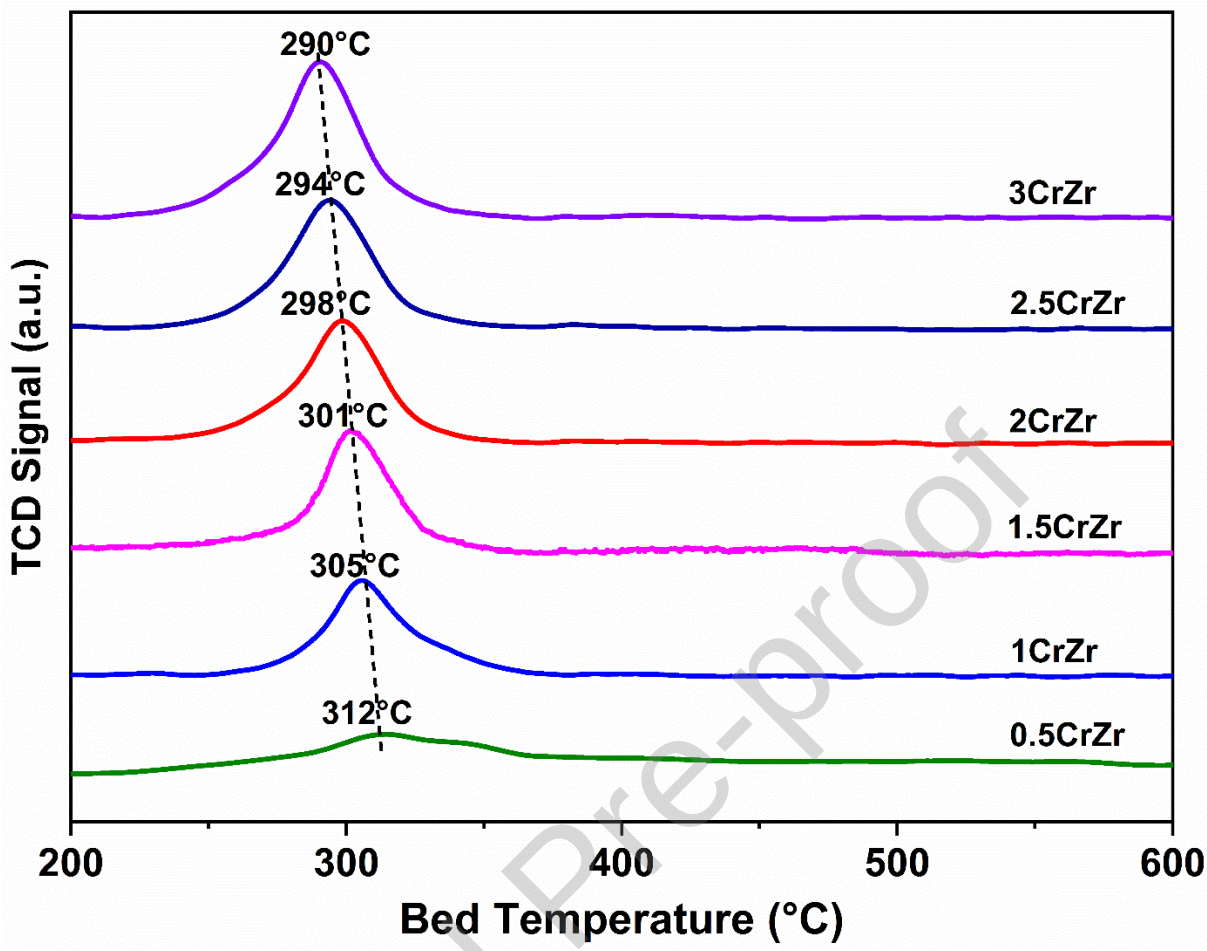

Figure 3: H_2 TPR profile of xCrZr catalyst showing the effect of metal oxide loading, x = 0.5, 1.0, 1.5, 2.0 2.5 and 3.0. The dotted line is used as a guide to show the decrease in T_{max} with loading.

The last set of catalyst were prepared to check the effect of potassium loading on the 2.5CrZr sample, and the H_2-TPR profiles are shown in Figure 4. Similar to a previous study, with an increase in the amount of potassium, the T_{max} of the sample gradually increases [49]. Specifically, the T_{max} increases from 294 ℃ for 2.5CrZr to 306 ℃ for 2.5Cr0.20K. However, the $H_2 - uptake$ initially increases when the potassium loading is increased from 2.5CrZr to 2.5Cr0.05K and then it starts decreasing with additional potassium loading. Since the amount of chromia is the same in these samples, the H/Cr molar ratio also follows the same trend, and the values are given in Table S7.

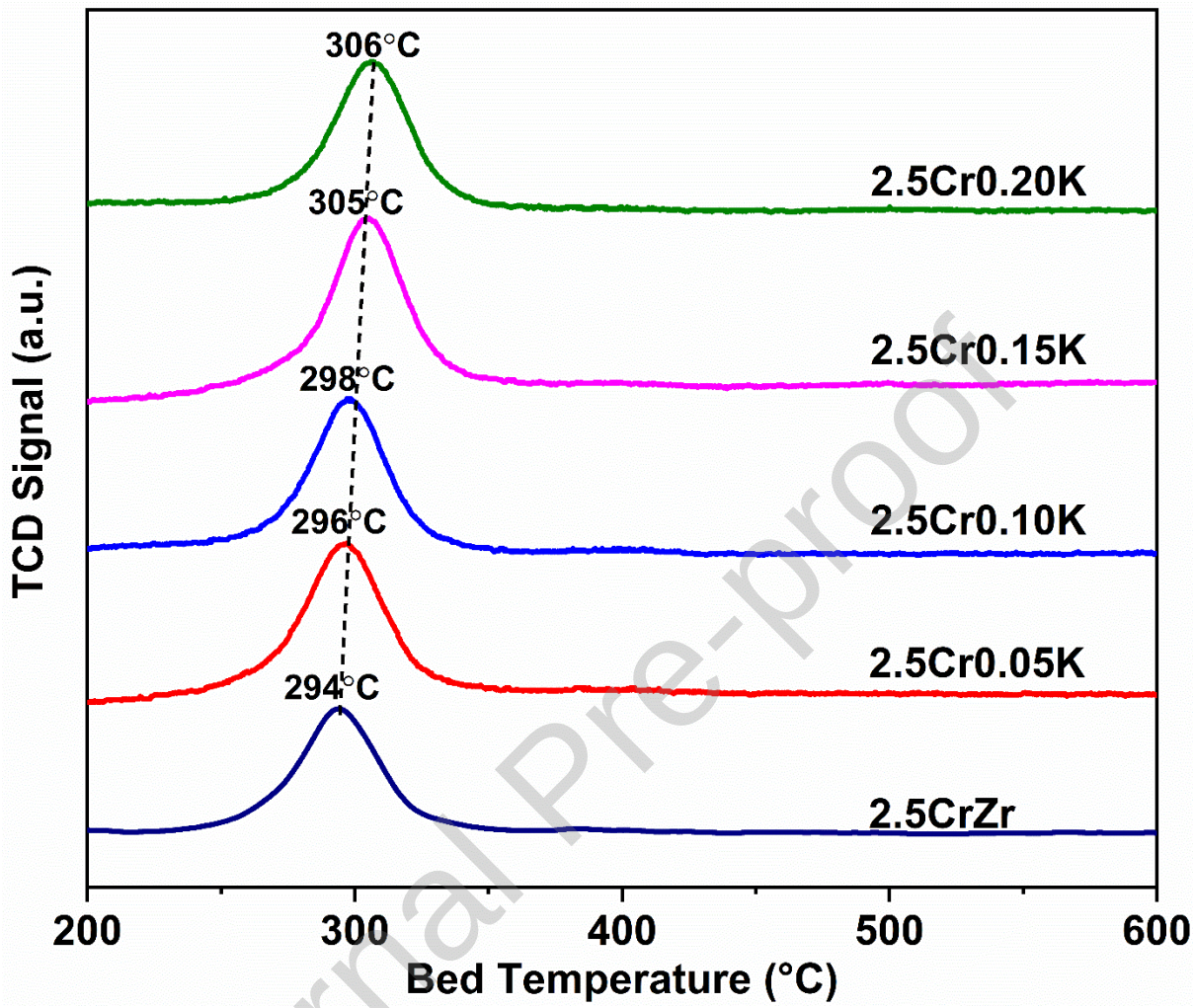

Figure 4: H_2 TPR profile of 2.5CrZr and 2.5CryK catalyst showing the effect of potassium addition, y = 0.05, 0.10, 0.15 and 0.20. The dotted line is used as a guide to show the increase in T_{max} with potassium amount.

3.5. XPS data

The XPS spectra of the freshly calcined 2MZr catalysts, M = Cr, Fe and V are shown in Figure 5. The spectra of the 2CrZr shows the presence of Cr^{+6} (579.08 and 588.68 eV) and Cr^{+3} (576.61 and 585.78eV) in the $2p_{3/2}$ and $2p_{1/2}$ regions [95]. The presence of this Cr^{+3} species in the calcined sample was not readily detected by UV-vis and Raman spectroscopy. It is only when the Cr^{+3} species was present as Cr_2O_3 was it seen in the UV-vis and Raman spectra. In contrast,

the H_2-TPR studies does give some indication of the presence of C^{+3} species, since the H/Cr ratio is less than 3. It appears that this Cr^{3+} species is strongly interacting with the support. Furthermore, since the H/Cr ratio decreases with chromia loading, it appears that the fraction of chromia present as irreducible chromia species in the calcined increases with chromia loading.

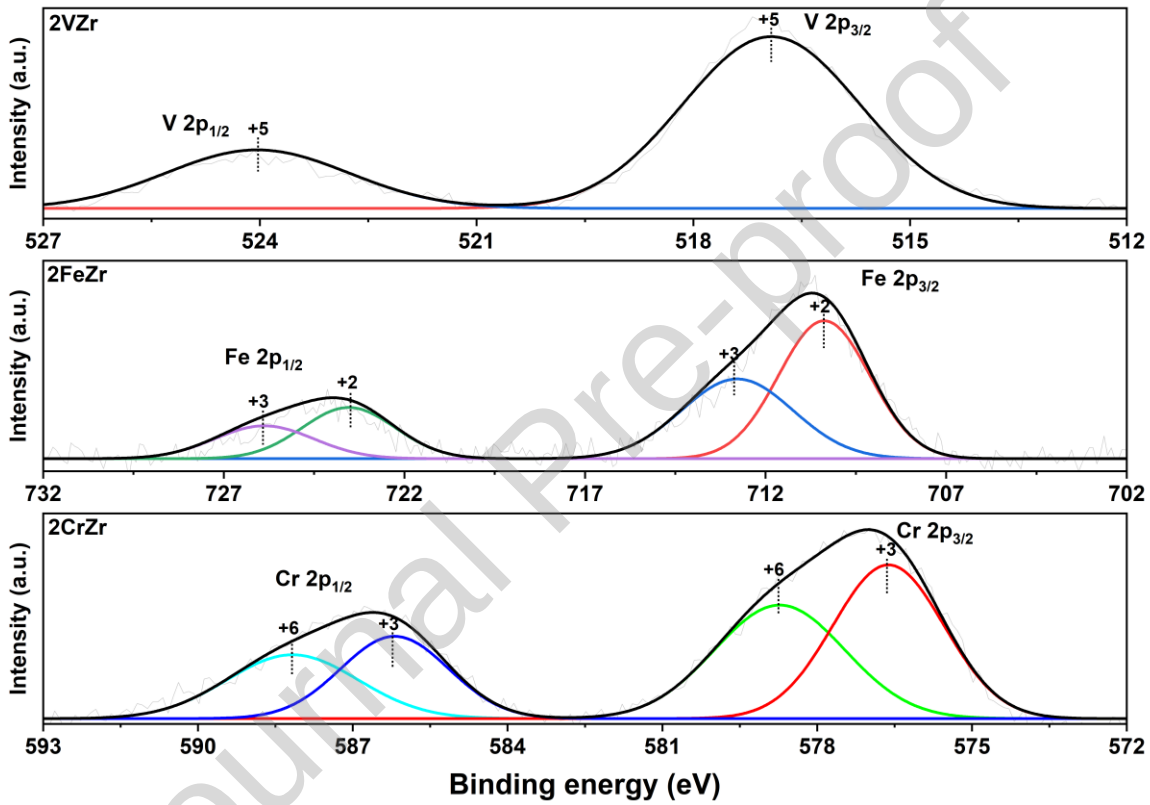

Figure 5: XPS spectra of freshly calcined samples of 2CrZr, 2FeZr and 2VZr.

The XPS spectra of the 2FeZr sample shows Fe^{+3} (712.78 and 725.88eV) and Fe^{+2} (710.37 and 723.54 eV) in the $2p_{3/2}$ and $2p_{1/2}$ regions [72]. The presence of Fe^{+2} species is evident and the H/Fe ratio of 2.4 determined from H_2-TPR confirms its presence. The XPS spectra of the calcined 2VZr sample reveals the presence of two peaks of V^{+5} species at 516.85 and 524.28 eV in the $2p_{3/2}$ and $2p_{1/2}$ regions, respectively [70].

3.6. Direct dehydrogenation of Propane

3.6.1. Effect of active metal

The C_3H_8 conversion and C_3H_6 yield of the PDH reaction at 550^{o}C over 2CrZr, 2VZr and 2FeZr are shown in Figure 6 as a function of TOS. Furthermore, the conversion and yield values were below equilibrium values (conversion = 75.9% and yield = 75.9%) at these operating conditions. The change in conversion and yields are noticeable and reproducible. Despite these variations it is evident that the trend in activity for the supported metal oxide is:

$$2CrZr > 2FeZr > 2VZr$$

Since the supported metal oxide species are molecularly dispersed, as shown by UV-vis and Raman spectroscopy, and the atomic weights are similar, it would be tempting to suggest that the TOF_{C3H8} and TOF_{C3H6} at 0.5 h during PDH follows the same trend. However, the H_2-TPR studies above reveal that the number of reducible sites is less than the total amount of chromia in the 2CrZr sample. A detailed study by de Rossi et al showed that the catalytically active species is formed from chromia present in the high oxidation state of Cr^{+6} and Cr^{+5} [44]. Hongfang et al also showed that catalytically active, lower oxidation state species (Cr^{+3}), are formed from higher oxidation state species (Cr^{+6}) during the PDH reaction [50]. Assuming that the reducible sites, as determined from H_2-TPR, correspond to these high oxidation state chromia species, the trend in TOFs will be the same as the trend in activity, but the TOF for 2CrZr will be higher. The TOFs for the three catalysts based on the H_2 uptake data are shown in Table S8. The TOF_{C3H8} at 550^{o}C at 0.5 h and a partial pressure of 0.075 atm of propane assuming differential reaction conditions for the three catalysts are: $6.17*10^{-3}$ sec^{-1} for 2CrZr, $3.89*10^{-3}$ sec^{-1} for 2FeZr and $2.90*10^{-3}$ sec^{-1} for 2VZr. Thus, for the same ZrO_2 support. the 2CrZr catalyst is the most active amongst the chosen transition metal oxide catalyst for the PDH reaction.

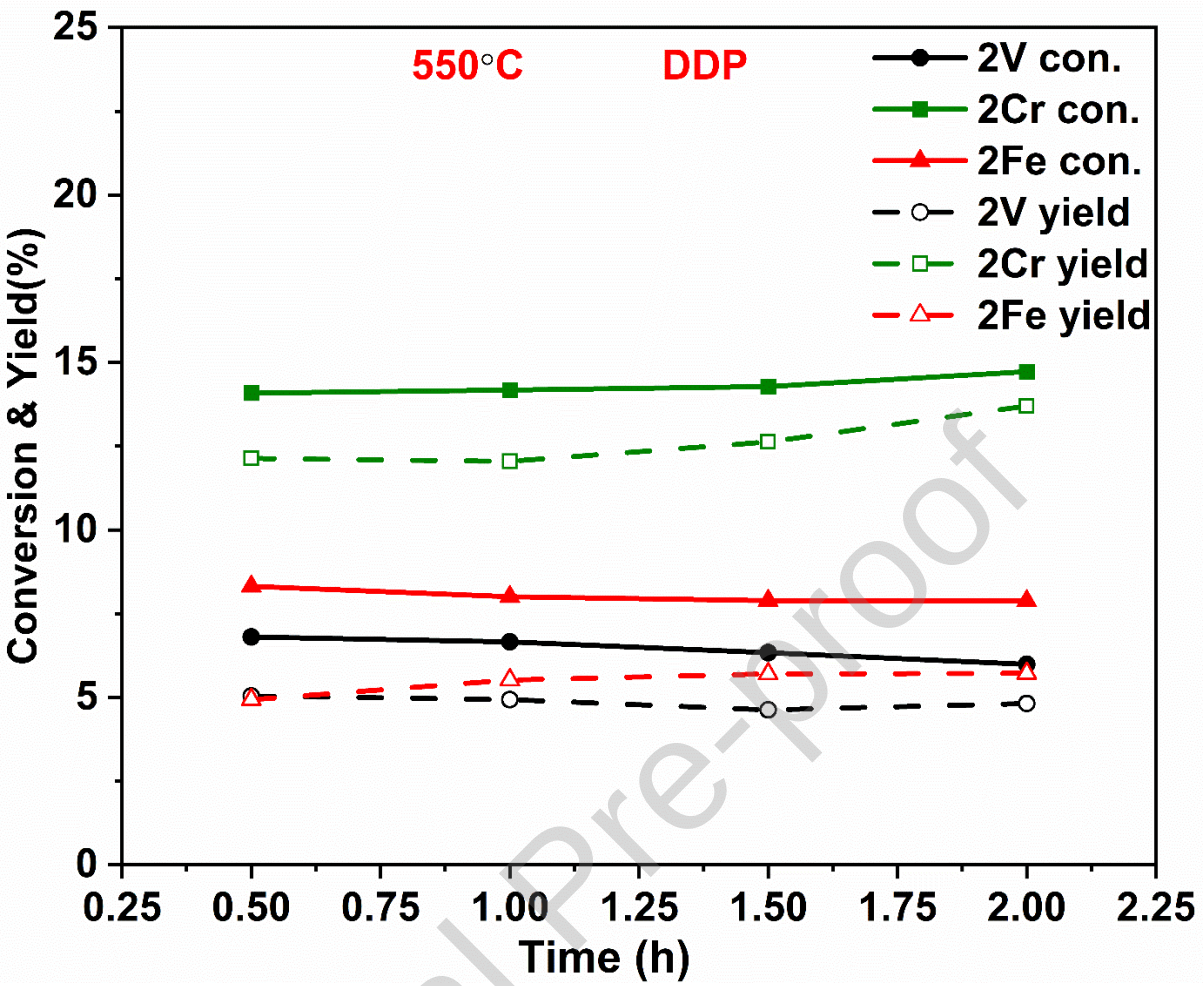

Figure 6: C_3H_8 conversion and C_3H_6 yield over three different catalysts (2VZr, 2CrZr and 2FeZr) during the PDH reaction at different TOS. Reaction conditions: Temperature 550°C, Total pressure = 1 atm, W=100 mg, W/FC3H8,0 = 16.59 g.h/mol, PC3H8,0 = 0.075 atm, balance N2.

3.6.2. Effect of support

Five different supports, Al_2O_3, CeO_2, Nb_2O_5, TiO_2 and ZrO_2, with the same loading of chromia (2%), were studied for the PDH reaction the same operating conditions to examine the effect of the support. All the 2CrS samples are less than monolayer loadings as revealed by Raman spectroscopy studies. The conversion and yield data for these catalysts have been shown in Table 1. The trend in propane conversion based on the values given in Table 1 is:

$$2CrZr > 2CrAl > 2CrCe > CrNb > 2CrTi$$

Using the same assumption that the reducible sites are active, the TOFs for the 2CrS catalysts are also shown in Table 1. Analysis of Table 1 reveals that ZrO_2 is the best support to use for carrying out the PDH reaction over supported chromia catalyst, whereas the TOFs of the other supported chromia catalysts show less than half the TOF value of 2CrZr. A previous study also suggests that ZrO_2 supported chromia catalyst provides higher TOF compared to Al_2O_3 and SiO_2 supports [43,44]. Furthermore, there appears to be no correlation between the T_{max} of these catalysts and the TOFs, suggesting that the binding of oxygen to the catalyst has no correlation with the PDH activity, unlike for the oxidative dehydrogenation (ODH) of methanol reaction over different supported vanadia catalysts [92]. This is consistent with the different reaction mechanisms that occur during PDH and ODH of methanol. During PDH reaction, a dual site and/or heterolytic mechanism is followed. The propane molecule gets adsorbed on the metal oxide catalyst surface terminally, which helps the abstraction of C-H bond. A hydrogen radical and a propyl radical adsorbed on the surface is formed. The propyl radical goes through another hydrogen abstraction which lead to propene gas and another hydrogen-radical. These two hydrogen-radicals forms hydrogen gas and disrobes from the catalytic surface [96,97]. In contrast, the ODH of propane occurs by the Mars van Krevelan mechanism and the involvement of the lattice oxygen is an integral part of the reaction mechanism [98]. Furthermore, there appears to be no co-relation between the TOF values and the surface coverage and the xCrZr catalysts are more active than the other supported chromia catalysts considered in the present study.

To address this exemplary behaviour of the ZrO_2 support a limited number of studies have taken place, primarily from the group of Kondratenko. Kondratenko and co-workers explained the effect of support by analysing the difference in the nature of the co-ordinated unsaturated sites (cus) that are formed on ZrO_2, TiO_2 and Al_2O_3 [99]. Furthermore, they suggested that the synergetic effect between Cr^{+3} and $Zr^{+4}{}_{cus}$ sites played an important role in the formation of

more active sites. For example, Han et al. [100] using state-of-the-art characterization techniques combined with kinetic studies and DFT calculations proposed that the chromium species improved the intrinsic activity of Zr_{cus} sites, which was the active site of the bare support. It appears that the support effect originates from the presence of these sites formed between the surface chromia and the $support_{cus}$ species in the supported chromia catalysts. Consequently, the Cr^{+3}-Zrcus site is the most active for the PDH reaction. Furthermore, the acidity and basicity of catalysts may play a significant role. For example, Fu et al showed that the acidity of the catalysts decreases with alkali addition [50]. This decrease in acidity decreases the side reaction, which lead to catalyst deactivation. However, the role of acidity of the 2CrS catalysts needs to be explored so that the effect of acidity of these catalysts on the PDH reaction can be established.

3.6.3. Effect of metal loading

The chromia amount was varied from 0.5% Cr to 3% Cr on the ZrO_2 support to identify the most suitable loading. The reactivity data shown in Figure 7 reveals that the propane conversion and propene yield increase with loading till 2.5% Cr. With additional chromia loading the conversion and yield decreases. The characterization studies revealed that the metal loadings chosen varied from sub monolayer to more than a monolayer coverage of chromia on this ZrO_2 support. The monolayer loading was determined to be between 2 and 2.5% chromia, since for 2.5% and higher loadings crystalline features of Cr_2O_3 were observed. Consequently, the variation of conversion and yield with loading can be explained by the presence of molecularly dispersed chromia species in the lower than 2.5% loading samples. Above monolayer loadings, at 2.5% and higher, crystalline Cr_2O_3 is present and all the chromia species are not available for the reaction. Accordingly, the conversion and yield decrease.

Similar variations of conversions and yields for the CO_2 assisted ODH reaction were also seen in a previous study [70]. For the O_2 assisted ODH reaction, a similar trend was also observed

by us for the same set of ZrO_2 supported chromia catalysts, which is shown in Figure S13. Furthermore, a strong correlation between the chromia loading and propane conversion for PDH and O_2 assisted ODH was observed for a series of Al_2O_3 supported chromia catalysts [101]. Thus, it appears that the monolayer chromia catalyst is the most active for these propane dehydrogenation and related reactions.

The conversion and yield based on the amount of reducible chromia present, as given in Table S10, is shown in Figure 8. The reducible amount of chromia is calculated based on nominal amount of metal loading. The conversion and yield increase as the amount of reducible chromia species increases and it is highest near the monolayer coverage. At above monolayer coverages the conversion and yield start to decrease. The TOF based on propane conversion and propene yield based on the amount of reducible species is shown in Table S10 of the supplementary information file. The TOF's as a function of chromia loading monotonically decrease suggesting that the reducible chromia species present at low loadings are more active than those present at higher loadings. Thus, the chromia species that are reducible appear to be the precursor for the active component for the dehydrogenation of propane. During reaction it is expected that the reducible chromia species is reduced to Cr^{+3}. Indeed. this is the case, as shown by XPS (Figure S14), where only Cr^{+3} is detected in the spent 2.5CrZr catalyst.

Table 1: C_3H_8 conversion, C_3H_6 yield and the corresponding TOFs for the PDH reaction at 550°C and partial pressure of C_3H_8 = 0.075 atm over 2CrS showing the effect of using different supports. S = Al_2O_3 (Al), CeO_2 (Ce), Nb_2O_5 (Nb), TiO_2 (Ti) and ZrO_2 (Zr).

Support	C_3H_8 Conversion		C_3H_6 Yield		$TOF_{C_3H_8} * 10^3 (sec^{-1})$		$TOF_{C_3H_6} * 10^3 (sec^{-1})$	
	0.5 h	2 h	0.5 h	2 h	0.5 h	2 h	0.5 h	2 h
2CrAl	6.08±0.26	4.77±0.19	3.17±0.09	3.17±0.09	2.65±0.11	2.08±0.08	1.38±0.04	1.38±0.04
2CrCe	3.29±0.11	3.34±0.09	3.27±0.10	3.32±0.15	1.43±0.05	1.45±0.04	1.42±0.04	1.44±0.07
2CrNb	3.27±0.18	3.05±0.13	1.85±0.11	1.62±0.10	1.42±0.08	1.33±0.06	0.81±0.05	0.71±0.04
2CrTi	2.35±0.06	1.55±0.09	1.04±0.14	0.93±0.10	1.02±0.02	0.67±0.04	0.45±0.06	0.40±0.04
2CrZr	14.17±0.50	14.72±0.20	12.05±0.23	13.70±0.21	6.17±0.22	6.41±0.08	5.24±0.10	5.96±0.09

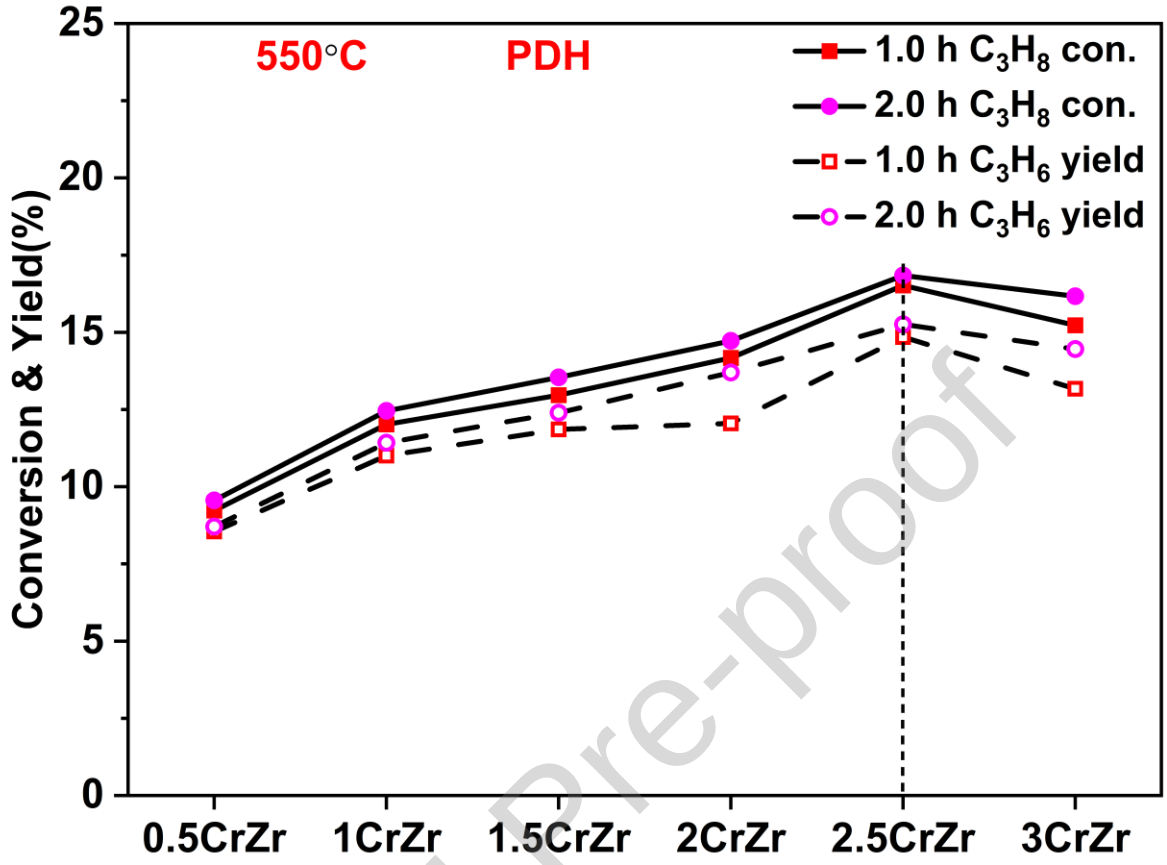

Figure 7: C_3H_8 conversion and C_3H_6 yield for the PDH over xCrZr catalyst showing the effect of chromia loading, x = 0.5, 1.0, 1.5, 2.0, 2.5 and 3.0. Reaction conditions: Temperature 550°C, Total pressure = 1 atm, W=100 mg, W/FC3H8,0 = 16.59 g.h/mol, PC3H8,0 = 0.075 atm, balance N2.

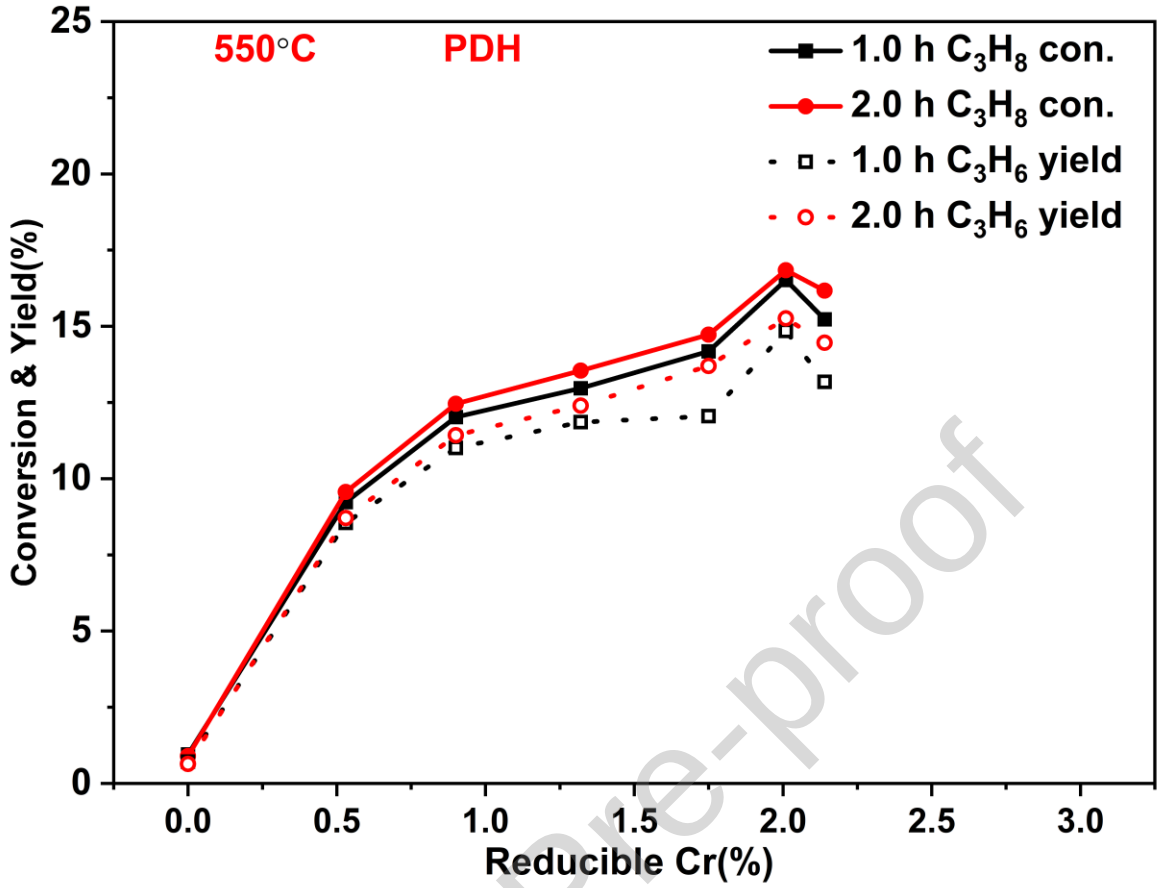

Figure 8: C_3H_8 conversion and C_3H_6 yield, at two TOS (1 h and 2 h), as a function of the reducible chromia amount in the xCrZr catalysts.

3.6.4. Effect of potassium loading

Four different amounts of potassium in the 2.5CrZr were tested for the PDH reaction and the results are shown in Figure 9. The reaction results clearly reveal a specific amount of potassium is required for improving the conversion and yield of the PDH reaction. Unfortunately, this amount was not captured in the previous study [49]. Relative to 2.5CrZr, the activity increases for the 2.5Cr0.05K catalyst, and with additional amount of potassium the activity of the catalysts decreases. The H_2 uptake for this set of catalyst, as mentioned in Table S7 of supporting information file, reveals that for 2.5Cr0.05K, the H/Cr ratio is maximum. This maximum H/Cr ratio suggests that relative to 2.5CrZr additional reducible chromia are formed.

It appears that potassium interacts with the ZrO_2 support is a way that reduces the formation of irreducible Cr^{+3} species. The consequence of this additional reducible chromia species is reflected in the increase in conversion and yield of the 2.5Cr0.05K catalyst. Furthermore, a more detailed analysis of Figure 9 shows that the propene selectivity ($X_{C_3H_6}/X_{C_3H_8}$) also increases. The TOFs based on propane conversion and propene formation is shown in Table S9. The TOFs have a similar trend as the H/Cr ratio, since it increases from 2.5CrZr to 2.5Cr0.05K, and further addition of K leads to a decrease.

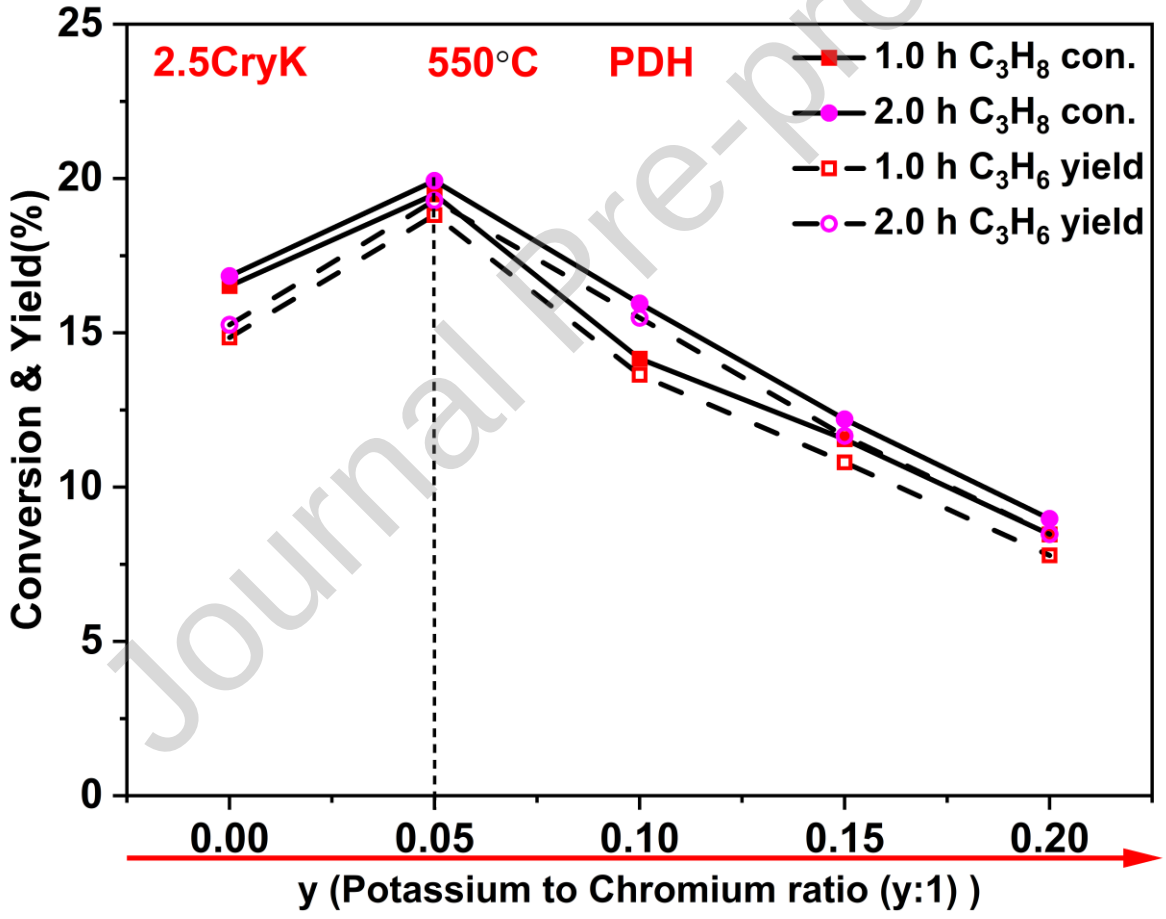

Figure 9: C_3H_8 conversion and C_3H_6 yield for the PDH over 2.5CryK catalyst showing the effect of increasing the K/Cr molar ratio, y = 0.05, 0.10, 0.15 and 0.20. Reaction conditions: Temperature 550°C, Total pressure = 1 atm, W=100 mg, W/FC3H8,0 = 16.59 g.h/mol, PC3H8,0 = 0.075 atm, balance N2.

3.6.5. Effect of operating temperature

It has been documented in literature that majority of the studies dealing with PDH have focused on a reaction temperature of 550°C [5,23,59,62,63], with nearly all investigations conducted within the reaction temperature range of 500-600°C [14,57,102,103] To determine a suitable reaction temperature regime, we examined the effect of reaction temperature between 500-600°C on two catalysts, 2.5CrZr and 2.5Cr0.05K. The propane conversion data for 2.5Cr0.05K is shown in Figure 10(A) and yield of propene is shown in Figure S15. The corresponding data for 2.5CrZr is given in Figure S16 of the supplementary information file. Both figures reveal that as the reaction temperature is increased to 550^{o}C, the conversion of propane and yield of propene also increased. The TOS data was also not significantly affected. However, above 550^{o}C, the TOS data showed a decrease in conversion and yield suggesting deactivation of the catalyst. We analysed the spent catalysts by Raman spectroscopy which is shown in Figure S17 of the supplementary information file. From Figure 10(B), it is apparent that the carbon peaks at 1350 and 1590 cm^{-1} are not evident at 540^{o}C, start appearing at 550^{o}C and then become prominent as the reaction temperature is increased further. Thus, the most suitable reaction temperature for PDH is 550°C or less for these supported chromia catalysts.

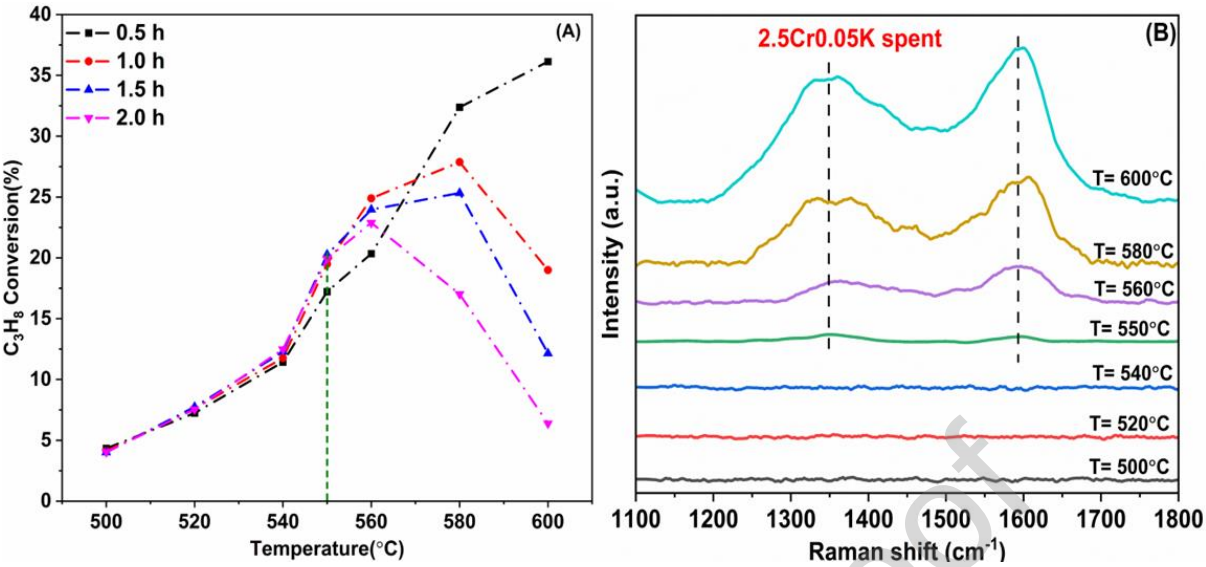

Figure 10: (A)C_3H_8 conversion for 2.5Cr0.05K catalyst at different TOS during PDH at reaction temperatures between 500-600°C. Reaction conditions: Total pressure = 1 atm, W=100 mg, W/FC3H8,0 = 16.59 g.h/mol, PC3H8,0 = 0.075 atm, balance N2. (B) Magnified Raman spectra of the spent 2.5Cr0.05K catalysts showing the effect of operating temperature T, where T = 500, 520, 540, 550, 5560, 580, and 600 °C.

3.6.6. Contact time study

To further increase the conversions, the effect of contact time was examined for 2.5Cr0.05K and 2.5CrZr. Figure 11 shows that the conversion of propane and yield of propene increases as the contact time increases and approaches a constant value of about 30% and 27% for 2.5Cr0.05K at 37.33 $g_{cat}.h/mol$. At all contact times the conversion and yields of 2.5Cr0.05K are more than 2.5CrZr, confirming that the promoted catalyst is more active than the unpromoted one under these conditions. Furthermore, as the contact time increases the difference between conversion and yield increases. Raman spectra of the spent 2.5Cr0.05K catalysts at different contact times shown in Figure S18 shows that the presence of carbon. Furthermore, the intensity of the carbon peaks increases with increase in contact time. Thus,

the increase in difference between the conversion and yield with contact time appears to be related to the increase in carbon formation.

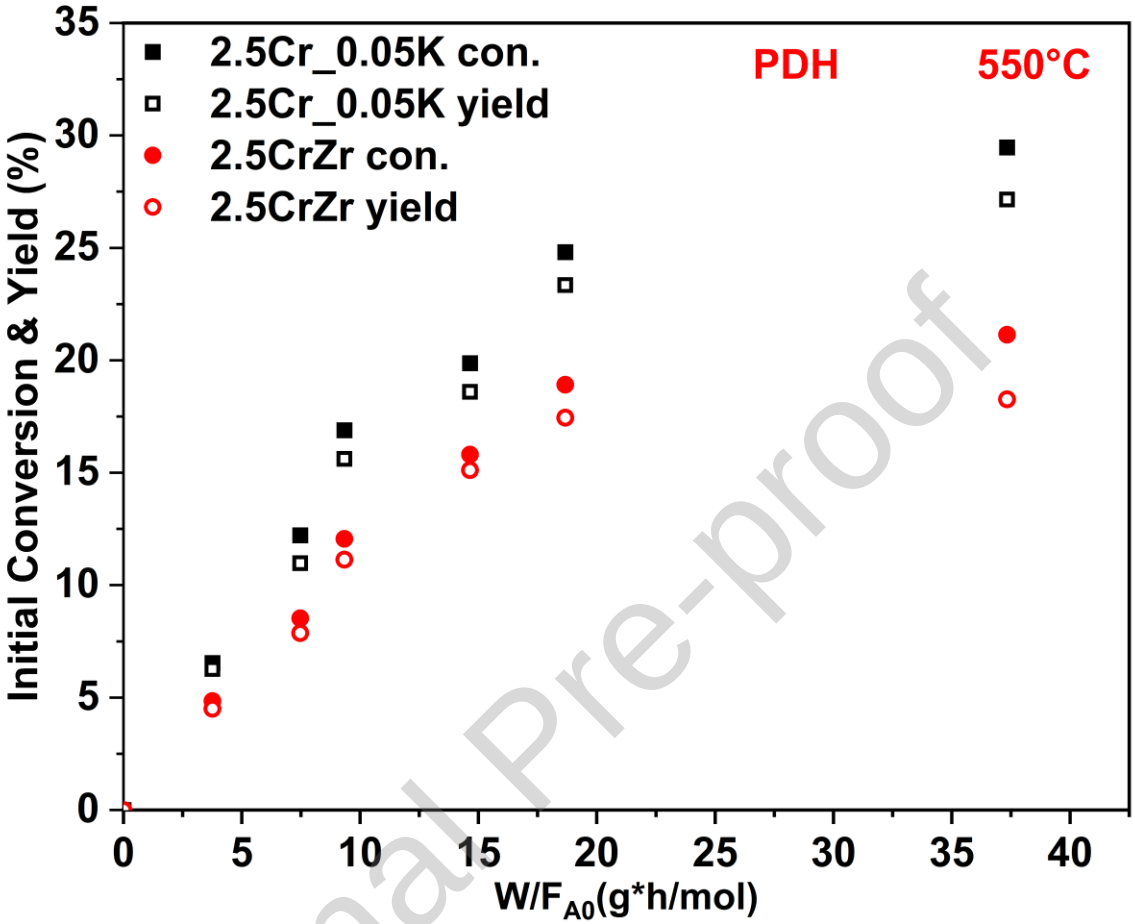

Figure 11: C_3H_8 conversion and C_3H_6 yield for the PDH over 2.5CrZr and 2.5Cr0.05K catalyst showing the effect of contact time. Reaction conditions: Temperature 550°C, Total pressure = 1 atm, W=100 mg, W/F$_{C3H8,0}$ = 0.00-37.33 $g_{cat}\,.\,h/mol$.

Several previous studies have reported Cr-based catalysts, a few of them are listed in Table 2. The operating conditions (temp. 550°C and pressure 1atm) were nearly similar. As we can see from the table below, the optimum Cr-metal loading varies from 2.5-20 wt%, which is mostly dependent on the support material. The GHSV varies from 3800- 18000 ($ml/g_{cat}.h$). In case of our catalyst, the optimum metal loading is 2.5%, which is lowest and the GHSV is highest among all. Despite being lowest loading and highest GHSV, our system shows comparable to all the catalysts.

Table 2: Comparison of catalytic performance of 2.5Cr0.05K with reported Cr-based catalysts at 550 ℃ and atmosphere pressure.

$\boldsymbol{Catalysts}$	$\boldsymbol{Cr}$ ($\boldsymbol{wt}$ %)	$\boldsymbol{GHSV}$ ($\boldsymbol{ml/g_{cat}.h}$)	$\boldsymbol{T}$ (℃)	$\boldsymbol{P_{C_3H_8}}$ ($\boldsymbol{atm}$)	$\boldsymbol{X_{C_3H_8}}$ **(%)**	$\boldsymbol{Y_{C_3H_6}}$ (%)
Cr5/SBA-1 [104]	5	9000	550	0.067	33	28.3
0.04Cr/SBA-1 [105]	4	9000	550	0.67	24.5	21.7
Cr20/Al_2O_3-n [106]	20	9000	550	0.67	33.7	31.8
Cr-3Ce-5Zr/Al_2O_3 [107]	20	2544	580	0.4	71	64
$Cr_{10}Zr_{90}/SiO_2$ [108]	3	11425	550	0.4	15	14.25
$CrZr_{30}/SiO_2$ [84]	3	4800	550	0.4	20	18
C_S-P/$CrZrO_x$ [109]	10	3790	550	0.4	30	28.5
Cr20/CMK-3 [110]	20	9000	550	0.067	22.4	20.8
2.5Cr-Ni/Al [111]	2.5	6000	550	0.1	40	36
ZCr10 [112]	10	12720	540	0.12	25	23.25
2.5Cr0.05K	**2.5**	**18000**	**550**	**0.033**	**30**	**27**

4. Conclusion

In this present study a promoted supported metal oxide catalyst for the PDH reaction was developed. Using ZrO_2 as the support and sub-monolayer loadings, Cr-oxide was found to be more active than Fe-oxide and V-oxide. Using the same metal loading of Cr to determine the effect of support, the ZrO_2 supported catalyst was found to be better than the other chromia supported catalysts. Subsequently, the chromia loading was varied on this ZrO_2 support, and the near-monolayer catalyst containing 2.5% Cr as metal (2.5CrZr), was the most active. Furthermore, the monolayer coverage on this ZrO_2 support was between 5.2 and 6.6 $atom_{Cr}/nm^2$. The performance of the 2.5CrZr was further improved by co-impregnating a limited amount of potassium. The best molar ratio of K/Cr was 0.05. It appears that this limited amount of K increased the amount of reducible chromia present in the 2.5Cr0.05K catalyst. The 2.5Cr0.05K was tested for the PDH reaction at different reaction temperatures and 550^{o}C was found to be the most suitable reaction temperature to carry out the reaction. At higher

reaction temperatures the catalyst deactivated. This deactivation appears to be related to carbon being deposited on the catalyst surface. Increasing the contact time facilitated an increase in the reactivity parameters and the highest conversions and yields achieved at 550°C and 37.33 $g_{cat}.h/mol$ were about 30% and 27%, respectively. Thus, using a systematic approach a suitable supported metal oxide catalyst for the PDH reaction.

Supplementary Information

Acknowledgement

The authors acknowledge IIT Kanpur and MoE for their continued support.

References

[1] H.A. Maddah, Polypropylene as a Promising Plastic: A Review, American Journal of Polymer Science 6 (2016) 1–11. https://doi.org/10.5923/j.ajps.20160601.01.

[2] J. Panming, W. Qiuying, Z. Chao, X. Yanhe, Alkylation of benzene with propene to produce cumene over a nickel/y-alumina catalyst, App Catal A: General 91 (1992) 125-129. https://doi.org/10.1016/0926-860X(92)85071-I

[3] G. Centi, R.K. Gbasseu, F. Tbifiro, Propane Ammoxidation to Acrylonitrile-An Overview, Catal Today 13 (1992) 661-666. https://doi.org/10.1016/0920-5861(92)80106-W

[4] U. Department of Energy, Chapter 6: Innovating Clean Energy Technologies in Advanced Manufacturing, 2015.

[5] S. Chen, X. Chang, G. Sun, T. Zhang, Y. Xu, Y. Wang, C. Pei, J. Gong, Propane dehydrogenation: Catalyst development, new chemistry, and emerging technologies, Chem Soc Rev 50 (2021) 3315–3354. https://doi.org/10.1039/d0cs00814a.

[6] X. Chen, N. Li, Y. Yang, C. Yang, H. Shan, Novel Propylene Production Route: Utilizing Hydrotreated Shale Oil as Feedstock via Two-Stage Riser Catalytic Cracking, Energy and Fuels 29 (2015) 7190–7195. https://doi.org/10.1021/acs.energyfuels.5b02076.

[7] A. Al-Douri, D. Sengupta, M.M. El-Halwagi, Shale gas monetization – A review of downstream processing to chemicals and fuels, J Nat Gas Sci Eng 45 (2017) 436–455. https://doi.org/10.1016/j.jngse.2017.05.016.

[8] R.B. Rostami, M. Ghavipour, Z. Di, Y. Wang, R.M. Behbahani, Study of coke deposition phenomena on the SAPO_34 catalyst and its effects on light olefin selectivity during the methanol to olefin reaction, RSC Adv 5 (2015) 81965–81980. https://doi.org/10.1039/c5ra11288e.

[9] J.J.H.B. Sattler, J. Ruiz-Martinez, E. Santillan-Jimenez, B.M. Weckhuysen, Catalytic dehydrogenation of light alkanes on metals and metal oxides, Chem Rev 114 (2014) 10613–10653. https://doi.org/10.1021/cr5002436.

[10] COMMODITY PRODUCTION COSTS PROPYLENE PRODUCTION FROM PROPANE (FIXED-BED REACTOR) PREMIUM EDITION | USA, 2024. www.intratec.us.

[11] F. Feng, H. Zhang, S. Chu, Q. Zhang, C. Wang, G. Wang, F. Wang, L. Bing, D. Han, Recent progress on the traditional and emerging catalysts for propane dehydrogenation, Journal of Industrial and Engineering Chemistry 118 (2023) 1–18. https://doi.org/10.1016/j.jiec.2022.11.001.

[12] G. Wang, X. Zhu, C. Li, Recent Progress in Commercial and Novel Catalysts for Catalytic Dehydrogenation of Light Alkanes, Chemical Record 20 (2020) 604–616. https://doi.org/10.1002/tcr.201900090.

[13] O.O. James, S. Mandal, N. Alele, B. Chowdhury, S. Maity, Lower alkanes dehydrogenation: Strategies and reaction routes to corresponding alkenes, Fuel Processing Technology 149 (2016) 239–255. https://doi.org/10.1016/j.fuproc.2016.04.016.

[14] J.H. Carter, T. Bere, J.R. Pitchers, D.G. Hewes, B.D. Vandegehuchte, C.J. Kiely, S.H. Taylor, G.J. Hutchings, Direct and oxidative dehydrogenation of propane: From catalyst design to industrial application, Green Chemistry 23 (2021) 9747–9799. https://doi.org/10.1039/d1gc03700e.

[15] W. Zhou, I.E. Wachs, C.J. Kiely, Nanostructural and chemical characterization of supported metal oxide catalysts by aberration corrected analytical electron microscopy, Curr Opin Solid State Mater Sci 16 (2012) 10–22. https://doi.org/10.1016/j.cossms.2011.06.001.

[16] M.A.B. Äares, Supported metal oxide and other catalysts for ethane conversion: a review, *Catalysis today* 51 (1999) 319-348. https://doi.org/10.1016/S0920-5861(99)00053-X

[17] I.E. Wachs, Raman and IR studies of surface metal oxide species on oxide supports: Supported metal oxide catalysts, *Catalysis today* 27 (1996) 437-455. https://doi.org/10.1016/0920-5861(95)00203-0

[18] F.E. Frey, W.F. Huppke, Equilibrium Dehydrogenation of Ethane, Propane, and the Butanes, *Industrial & Engineering Chemistry* 25 (1933): 54-59. https://pubs.acs.org/sharingguidelines.

[19] M.M. Bhasin, J.H. Mccain, B. V Vora, T. Imai, P.R. Pujadó, Dehydrogenation and oxydehydrogenation of paraffins to olefins, App Catal A: General 221 (2001) 397-419. https://doi.org/10.1016/S0926-860X(01)00816-X

[20] G. Liu, Z.J. Zhao, T. Wu, L. Zeng, J. Gong, Nature of the Active Sites of VOx/Al2O3 Catalysts for Propane Dehydrogenation, ACS Catal 6 (2016) 5207–5214. https://doi.org/10.1021/acscatal.6b00893.

[21] C. Xiong, S. Chen, P. Yang, S. Zha, Z.J. Zhao, J. Gong, Structure-Performance Relationships for Propane Dehydrogenation over Aluminum Supported Vanadium Oxide, ACS Catal 9 (2019) 5816–5827. https://doi.org/10.1021/acscatal.8b04701.

[22] C.T. Shao, W.Z. Lang, X. Yan, Y.J. Guo, Catalytic performance of gallium oxide based-catalysts for the propane dehydrogenation reaction: effects of support and loading amount, RSC Adv 7 (2017) 4710–4723. https://doi.org/10.1039/c6ra27204e.

[23] D. Zhao, X. Tian, D.E. Doronkin, S. Han, V.A. Kondratenko, J.D. Grunwaldt, A. Perechodjuk, T.H. Vuong, J. Rabeah, R. Eckelt, U. Rodemerck, D. Linke, G. Jiang, H. Jiao, E. V. Kondratenko, In situ formation of ZnOx species for efficient propane dehydrogenation, Nature 599 (2021) 234–238. https://doi.org/10.1038/s41586-021-03923-3.

[24] B. Hu, N.M. Schweitzer, G. Zhang, S.J. Kraft, D.J. Childers, M.P. Lanci, J.T. Miller, A.S. Hock, Isolated FeII on silica as a selective propane dehydrogenation catalyst, ACS Catal 5 (2015) 3494–3503. https://doi.org/10.1021/acscatal.5b00248.

[25] N. Jeon, H. Choe, B. Jeong, Y. Yun, Cu-promoted zirconia catalysts for non-oxidative propane dehydrogenation, Appl Catal A Gen 586 (2019). https://doi.org/10.1016/j.apcata.2019.117211.

[26] S.K. Matam, C. Moffat, P. Hellier, M. Bowker, I.P. Silverwood, C.R.A. Catlow, S. David Jackson, J. Craswell, P.P. Wells, S.F. Parker, E.K. Gibson, Investigation of moox/al2o3 under cyclic operation for oxidative and non-oxidative dehydrogenation of propane, Catalysts 10 (2020) 1–13. https://doi.org/10.3390/catal10121370.

[27] S. Tan, L.B. Gil, N. Subramanian, D.S. Sholl, S. Nair, C.W. Jones, J.S. Moore, Y. Liu, R.S. Dixit, J.G. Pendergast, Catalytic propane dehydrogenation over In2O3-Ga2O3 mixed oxides, Appl Catal A Gen 498 (2015) 167–175. https://doi.org/10.1016/j.apcata.2015.03.020.

[28] J. Zhu Chen, A. Talpade, G.A. Canning, P.R. Probus, F.H. Ribeiro, A.K. Datye, J.T. Miller, Strong metal-support interaction (SMSI) of Pt/CeO2 and its effect on propane dehydrogenation, Catal Today 371 (2021) 4–10. https://doi.org/10.1016/j.cattod.2020.06.075.

[29] H. Xiong, S. Lin, J. Goetze, P. Pletcher, H. Guo, L. Kovarik, K. Artyushkova, B.M. Weckhuysen, A.K. Datye, Thermally Stable and Regenerable Platinum–Tin Clusters for Propane Dehydrogenation Prepared by Atom Trapping on Ceria, Angewandte Chemie - International Edition 56 (2017) 8986–8991. https://doi.org/10.1002/anie.201701115.

[30] S. Tan, B. Hu, W.G. Kim, S.H. Pang, J.S. Moore, Y. Liu, R.S. Dixit, J.G. Pendergast, D.S. Sholl, S. Nair, C.W. Jones, Propane Dehydrogenation over Alumina-Supported Iron/Phosphorus Catalysts: Structural Evolution of Iron Species Leading to High Activity and Propylene Selectivity, ACS Catal 6 (2016) 5673–5683. https://doi.org/10.1021/acscatal.6b01286.

[31] K. Searles, K.W. Chan, J.A. Mendes Burak, D. Zemlyanov, O. Safonova, C. Copéret, Highly Productive Propane Dehydrogenation Catalyst Using Silica-Supported Ga-Pt Nanoparticles Generated from Single-Sites, J Am Chem Soc 140 (2018) 11674–11679. https://doi.org/10.1021/jacs.8b05378.

[32] N.M. Schweitzer, B. Hu, U. Das, H. Kim, J. Greeley, L.A. Curtiss, P.C. Stair, J.T. Miller, A.S. Hock, Propylene hydrogenation and propane dehydrogenation by a single-site Zn2+ on silica catalyst, ACS Catal 4 (2014) 1091–1098. https://doi.org/10.1021/cs401116p.

[33] V. V. Kaichev, Y.A. Chesalov, A.A. Saraev, A.M. Tsapina, A Mechanistic Study of Dehydrogenation of Propane over Vanadia-Titania Catalysts, Journal of Physical Chemistry C 123 (2019) 19668–19680. https://doi.org/10.1021/acs.jpcc.9b04991.

[34] Y. Zhang, Y. Zhao, T. Otroshchenko, H. Lund, M.M. Pohl, U. Rodemerck, D. Linke, H. Jiao, G. Jiang, E. V. Kondratenko, Control of coordinatively unsaturated Zr sites in ZrO2 for efficient C–H bond activation, Nat Commun 9 (2018). https://doi.org/10.1038/s41467-018-06174-5.

[35] L.R. Mentasty, O.F. Gorriz, L.E. Cadus, Chromium oxide supported on different Al2O3 supports: Catalytic propane dehydrogenation, Ind Eng Chem Res 38 (1999) 396–404. https://doi.org/10.1021/ie9802562.

[36] A.L. Guimarães, L.C. Dieguez, M. Schmal, Surface sites of Pd/CeO2/Al2O3 catalysts in the partial oxidation of propane, Journal of Physical Chemistry B 107 (2003) 4311–4319. https://doi.org/10.1021/jp0270194.

[37] M. Cherian, M.S. Rao, A.M. Hirt, I.E. Wachs, G. Deo, Oxidative dehydrogenation of propane over supported chromia catalysts: Influence of oxide supports and chromia loading, J Catal 211 (2002) 482–495. https://doi.org/10.1006/jcat.2002.3759.

[38] P. Viparelli, P. Ciambelli, L. Lisi, G. Ruoppolo, G. Russo, J. Claude Volta, Oxidative dehydrogenation of propane over vanadium and niobium oxides supported catalysts, App catal A: General 184 (1999) 291-301. https://doi.org/10.1016/S0926-860X(99)00104-0

[39] M. Cherian, M. Someswara Rao, G. Deo, Niobium oxide as support material for the oxidative dehydrogenation of propane, Catal Today 78 (2003) 397-409. https://doi.org/10.1016/S0920-5861(02)00306-1

[40] Y. Zhang, Y. Yu, Y. Dai, Y. Zhang, Q. Liu, D. Xiong, L. Bao, Q. Wu, D. Shi, K. Chen, Y. Li, G. Jiang, E. V. Kondratenko, H. Li, Regulating the C-H Bond Activation Pathway over ZrO2 via Doping Engineering for Propane Dehydrogenation, ACS Catal 13 (2023) 6893–6904. https://doi.org/10.1021/acscatal.3c01002.

[41] A. Perechodjuk, Y. Zhang, V.A. Kondratenko, U. Rodemerck, D. Linke, S. Bartling, C.R. Kreyenschulte, G. Jiang, E. V. Kondratenko, The effect of supported Rh, Ru, Pt or Ir nanoparticles on activity and selectivity of ZrO2-based catalysts in non-oxidative dehydrogenation of propane, Appl Catal A Gen 602 (2020). https://doi.org/10.1016/j.apcata.2020.117731.

[42] A. Mukherjee, C. Samanta, A. Bordoloi, On-purpose production of light olefins through oxidative dehydrogenation: An overview of recent developments, ChemCatChem (2024). https://doi.org/10.1002/cctc.202401187.

[43] S. De Rossi, G. Ferraris, S. Fremiotti, V. Indovina, A. Cimino, Isobutane dehydrogenation on chromia/zirconia catalysts, App Catal A: General 106 (1993) 125-141. https://doi.org/10.1016/0926-860X(93)80160-R

[44] S. De Rossi, M.P. Casaletto, G. Ferraris, A. Cimino, G. Minelli, Chromia/zirconia catalysts with Cr content exceeding the monolayer. A comparison with chromia/alumina and chromia/silica for isobutane dehydrogenation, App Catal A: General 167 (1998) 257-270. https://doi.org/10.1016/S0926-860X(97)00315-3

[45] T.P. Otroshchenko, U. Rodemerck, D. Linke, E. V. Kondratenko, Synergy effect between Zr and Cr active sites in binary CrZrOx or supported CrOx/LaZrOx: Consequences for catalyst activity, selectivity and durability in non-oxidative propane dehydrogenation, J Catal 356 (2017) 197–205. https://doi.org/10.1016/j.jcat.2017.10.012.

[46] H. Zhou, J. Gong, B. Xu, L. Yu, Y. Fan, PtSnNa@SUZ-4-catalyzed propane dehydrogenation, Appl Catal A Gen 527 (2016) 30–35. https://doi.org/10.1016/j.apcata.2016.08.017.

[47] A. Van Assche, C. Especel, A. Le Valant, F. Epron, Effect of potassium and platinum contents on catalytic performance of Pt/Al2O3 monometallic catalysts for propane dehydrogenation, Molecular Catalysis 517 (2022). https://doi.org/10.1016/j.mcat.2021.112059.

[48] L. Cai, Y. Zhao, X. Tian, D. Qin, C. Wei, X. Cai, W. Chu, W. Yang, Well-dispersed monolayer CrOx/Silicalite-1 catalysts for efficient propane dehydrogenation, Chemical Engineering Journal 494 (2024). https://doi.org/10.1016/j.cej.2024.152925.

[49] M.G. Cutrufello, S. De Rossi, I. Ferino, R. Monaci, E. Rombi, V. Solinas, Preparation, characterisation and activity of chromia-zirconia catalysts for propane dehydrogenation, in: Thermochim Acta, 2005: pp. 62–68. https://doi.org/10.1016/j.tca.2005.01.017.

[50] H. Fu, W. Qian, H. Zhang, H. Ma, W. Ying, Different alkali metals promoted Cr/Al2O3 catalysts for propane dehydrogenation, Fuel 342 (2023). https://doi.org/10.1016/j.fuel.2023.127774.

[51] S.M. Ai-Zahrani, Propane Oxydehydrogenation to Propylene Over Molybdenum-based Catalysts, *Journal of King Saud University-Engineering Sciences* 16 (2004) 203-213. https://doi.org/10.1016/S1018-3639(18)30787-6

[52] S.N.R. Inturi, M. Suidan, P.G. Smirniotis, Influence of synthesis method on leaching of the Cr-TiO2 catalyst for visible light liquid phase photocatalysis and their stability, Appl Catal B 180 (2016) 351–361. https://doi.org/10.1016/j.apcatb.2015.05.046.

[53] S. De Rossi, G. Ferraris, S. Fremiotti, A. Cimino, V. Indovina, Propane dehydrogenation on chromia/zirconia catalysts, App Catal A: General 81 (1992) 113-132. https://doi.org/10.1016/0926-860X(92)80264-D

[54] O.F. Gorriz, L.E.C. Âs, Supported chromium oxide catalysts using metal carboxylate complexes: dehydrogenation of propane, App Catal A: General 180 (1999) 247-260. https://doi.org/10.1016/S0926-860X(98)00344-5

[55] L.E. Briand, O.P. Tkachenko, M. Guraya, X. Gao, I.E. Wachs, W. Grünert, Surface-Analytical Studies of Supported Vanadium Oxide Monolayer Catalysts, Journal of Physical Chemistry B 108 (2004) 4823–4830. https://doi.org/10.1021/jp037675j.

[56] M.A. Bafiares, X. Gao, J.L.G. Fierro, I.E. Wachs, Partial Oxidation of Ethane over Monolayers of Vanadium Oxide. Effect of the Support and Surface Coverage, Studies in Surface Science and Catalysis 110 (1997) 295-304. https://doi.org/10.1016/S0167-2991(97)80990-1

[57] D. Shee, A. Sayari, Light alkane dehydrogenation over mesoporous Cr2O 3/Al2O3 catalysts, Appl Catal A Gen 389 (2010) 155–164. https://doi.org/10.1016/j.apcata.2010.09.013.

[58] I.E. Wachs, Catalysis science of supported vanadium oxide catalysts, Dalton Transactions 42 (2013) 11762–11769. https://doi.org/10.1039/c3dt50692d.

[59] A. Węgrzyniak, S. Jarczewski, A. Wach, E. Hędrzak, P. Kuśtrowski, P. Michorczyk, Catalytic behaviour of chromium oxide supported on CMK-3 carbon replica in the dehydrogenation propane to propene, Appl Catal A Gen 508 (2015) 1–9. https://doi.org/10.1016/j.apcata.2015.10.002.

[60] I.E. Wachs, Infrared spectroscopy of supported metal oxide catalysts, *Colloids and Surfaces A: Physicochemical and Engineering Aspects* 105 (1995) 143-149. https://doi.org/10.1016/0927-7757(95)03325-5

[61] I.E. Wachs, Number of surface sites and turnover frequencies for oxide catalysts, J Catal 405 (2022) 462–472. https://doi.org/10.1016/j.jcat.2021.12.032.

[62] C. Chen, S. Zhang, Z. Wang, Z.Y. Yuan, Ultrasmall Co confined in the silanols of dealuminated beta zeolite: A highly active and selective catalyst for direct dehydrogenation of propane to propylene, J Catal 383 (2020) 77–87. https://doi.org/10.1016/j.jcat.2019.12.037.

[63] P.P. Li, W.Z. Lang, K. Xia, L. Luan, X. Yan, Y.J. Guo, The promotion effects of Ni on the properties of Cr/Al catalysts for propane dehydrogenation reaction, Appl Catal A Gen 522 (2016) 172–179. https://doi.org/10.1016/j.apcata.2016.05.007.

[64] Y. Zhang, Y. Zhao, T. Otroshchenko, S. Han, H. Lund, U. Rodemerck, D. Linke, H. Jiao, G. Jiang, E. V. Kondratenko, The effect of phase composition and crystallite size on activity and selectivity of ZrO2 in non-oxidative propane dehydrogenation, J Catal 371 (2019) 313–324. https://doi.org/10.1016/j.jcat.2019.02.012.

[65] J.J.H.B. Sattler, I.D. González-Jiménez, A.M. Mens, M. Arias, T. Visser, B.M. Weckhuysen, Operando uv-vis spectroscopy of a catalytic solid in a pilot-scale reactor: Deactivation of a crox/al2o3 propane dehydrogenation catalyst, Chemical Communications 49 (2013) 1518–1520. https://doi.org/10.1039/c2cc38978a.

[66] S. Tan, S.J. Kim, J.S. Moore, Y. Liu, R.S. Dixit, J.G. Pendergast, D.S. Sholl, S. Nair, C.W. Jones, Propane Dehydrogenation over In2O3-Ga2O3-Al2O3 Mixed Oxides, ChemCatChem 8 (2016) 214–221. https://doi.org/10.1002/cctc.201500916.

[67] T. V. Malleswara Rao, G. Deo, J.M. Jehng, I.E. Wachs, In situ UV-Vis-NIR diffuse reflectance and raman spectroscopy and catalytic activity studies of propane oxidative dehydrogenation over supported CrO 3/ZrO 2 catalysts, Langmuir 20 (2004) 7159–7165. https://doi.org/10.1021/la049590v.

[68] M. Xiao, Y. Li, Y. Lu, Z. Ye, Synthesis of ZrO2:Fe nanostructures with visible-light driven H2 evolution activity, J Mater Chem A Mater 3 (2015) 2701–2706. https://doi.org/10.1039/c4ta05931j.

[69] J. Liu, Z. Zhao, C. Xu, A. Duan, G. Jiang, J. Gao, W. Lin, I.E. Wachs, In-situ UV-Raman study on soot combustion over TiO2 or ZrO 2-supported vanadium oxide catalysts, Sci China B Chem 51 (2008) 551–561. https://doi.org/10.1007/s11426-008-0027-2.

[70] R. Singh, S.C. Nayak, R. Singh, G. Deo, O2 and CO2 assisted oxidative dehydrogenation of propane using ZrO2 supported vanadium and chromium oxide catalysts, Catal Today 432 (2024). https://doi.org/10.1016/j.cattod.2024.114617

[71] M. Németh, D. Srankó, J. Károlyi, F. Somodi, Z. Schay, G. Sáfrán, I. Sajó, A. Horváth, Na-promoted Ni/ZrO2 dry reforming catalyst with high efficiency: Details of Na2O-ZrO2-Ni interaction controlling activity and coke formation, Catal Sci Technol 7 (2017) 5386–5401. https://doi.org/10.1039/c7cy01011g.

[72] J. Kumar Prabhakar, P.A. Apte, G. Deo, Exploring optimal total metal loading of Ni3Fe/Al2O3 catalyst for CO2 methanation and its kinetic model, Fuel 367 (2024). https://doi.org/10.1016/j.fuel.2024.131447.

[73] C.L. Pieck, M.A. Bañares, J.L.G. Fierro, Propane oxidative dehydrogenation on VOx/ZrO2 catalysts, J Catal 224 (2004) 1–7. https://doi.org/10.1016/j.jcat.2004.02.024.

[74] A.B. Gaspar, L.C. Dieguez, Distribution of chromium species in catalysts supported on ZrO 2/Al2O3 and performance in dehydrogenation, J Catal 220 (2003) 309–316. https://doi.org/10.1016/S0021-9517(03)00297-5.

[75] K.V.R. Chary, C.P. Kumar, D. Naresh, T. Bhaskar, Y. Sakata, Characterization and reactivity of Al2O3-ZrO 2 supported vanadium oxide catalysts, J Mol Catal A Chem 243 (2006) 149–157. https://doi.org/10.1016/j.molcata.2005.07.036.

[76] A. Gervasini, C. Messi, A. Ponti, S. Cenedese, N. Ravasio, Nanodispersed Fe oxide supported catalysts with tuned properties, Journal of Physical Chemistry C 112 (2008) 4635–4642. https://doi.org/10.1021/jp710742g.

[77] T. Herranz, S. Rojas, F.J. Pérez-Alonso, M. Ojeda, P. Terreros, J.L.G. Fierro, Carbon oxide hydrogenation over silica-supported iron-based catalysts. Influence of the preparation route, Appl Catal A Gen 308 (2006) 19–30. https://doi.org/10.1016/j.apcata.2006.04.007.

[78] J. Kumar Prabhakar, P.A. Apte, G. Deo, The kinetics of Ni/Al2O3 and Ni-Fe/Al2O3 catalysts for the CO2 methanation reaction and the reasons for promotion, Chemical Engineering Journal 471 (2023). https://doi.org/10.1016/j.cej.2023.144252.

[79] D. Pandey, K. Ray, R. Bhardwaj, S. Bojja, K.V.R. Chary, G. Deo, Promotion of unsupported nickel catalyst using iron for CO2 methanation, Int J Hydrogen Energy 43 (2018) 4987–5000. https://doi.org/10.1016/j.ijhydene.2018.01.144.

[80] D. Pandey, K. Ray, R. Bhardwaj, S. Bojja, K.V.R. Chary, G. Deo, Promotion of unsupported nickel catalyst using iron for CO2 methanation, Int J Hydrogen Energy 43 (2018) 4987–5000. https://doi.org/10.1016/j.ijhydene.2018.01.144.

[81] M. Cherian, S. Rao, W.-T. Yang, J.-M. Jehng, A.M. Hirt, G. Deo, Oxidative dehydrogenation of propane over Cr2 O3 /Al2O3 and Cr2O3 catalysts: effects of loading, precursor and surface area, App Catal A: General 233 (2002) 21-33. https://doi.org/10.1016/S0926-860X(02)00132-1

[82] N.E. Fouad, H. Knözinger, M.I. Zaki, Chromia on Silica and Alumina Catalysts: CO Oxidation Activity, Zeitschrift für Physikalische Chemie 203 (1998) 131-142. https://doi.org/10.1524/zpch.1998.203.Part_1_2.131

[83] S. Sagadevan, M.R. Johan, J.A. Lett, Fabrication of reduced graphene oxide/CeO2 nanocomposite for enhanced electrochemical performance, Appl Phys A Mater Sci Process 125 (2019). https://doi.org/10.1007/s00339-019-2625-6.

[84] S. Han, T. Otroshchenko, D. Zhao, H. Lund, N. Rockstroh, T.H. Vuong, J. Rabeah, U. Rodemerck, D. Linke, M. Gao, G. Jiang, E. V. Kondratenko, The effect of ZrO2 crystallinity in CrZrOx/SiO2 on non-oxidative propane dehydrogenation, Appl Catal A Gen 590 (2020). https://doi.org/10.1016/j.apcata.2019.117350.

[85] P. Bouvier, G. Lucazeau, Raman spectra and vibrational analysis of nanometric tetragonal zirconia under high pressure, Journal of Physics and Chemistry of Solids, 61 (2000) 569-578. https://doi.org/10.1016/S0022-3697(99)00242-5

[86] Z. Liu, L. Zhang, S. Ren, Y. Zhao, S. Agathopoulos, H. Lu, B. Peng, L. Yin, L. Deng, Stability and reactivity of zirconium diboride in intermediate-temperature hydrothermal conditions: A comprehensive analysis, Mater Today Commun 41 (2024). https://doi.org/10.1016/j.mtcomm.2024.110482.

[87] F.D. Hardcastle, I.E. Wachs, RAMAN SPECTROSCOPY OF CHROMIUM OXIDE SUPPORTED ON Al2O3, TiO2 AND Si02: A COMPARATIVE STUDY, J. Mol. Catal 46 (1988) 173-186. https://doi.org/10.1016/0304-5102(88)85092-2

[88] J.-M. Jehng, I.E. Wachs, Niobium Oxide Solution Chemistry, Journal of Raman Spectroscopy 22 (1991) 83-89. **https://doi.org/10.1002/jrs.1250220207**.

[89] J.F.S. de Oliveira, D.P. Volanti, J.M.C. Bueno, A.P. Ferreira, Effect of CO2 in the oxidative dehydrogenation reaction of propane over Cr/ZrO2 catalysts, Appl Catal A Gen 558 (2018) 55–66. https://doi.org/10.1016/j.apcata.2018.03.020.

[90] B.M. Weckhuysen, I.E. Wachs, R.A. Schoonheydt, Surface Chemistry and Spectroscopy of Chromium in Inorganic Oxides, Chem. Rev. 96 (1996) 3327-3350. https://doi.org/10.1021/cr940044o

[91] E. Rombi, D. Gazzoli, M.G. Cutrufello, S. De Rossi, I. Ferino, Modifications induced by potassium addition on chromia/alumina catalysts and their influence on the catalytic activity for the oxidative dehydrogenation of propane, Appl Surf Sci 256 (2010) 5576–5580. https://doi.org/10.1016/j.apsusc.2009.12.151.

[92] G. Deo, I.E. Wachs, Reactivity of Supported Vanadium Oxide Catalysts The Partial Oxidation of Methanol, J Catal 146 (1994) 323-334. https://doi.org/10.1006/jcat.1994.1071

[93] M. Valenzuela, P. Bosch, J. Jiménez-Becerrill, O. Quiroz, A. Páez, Preparation, characterization and photocatalytic activity of ZnO, Fe2O3 and ZnFe2O3, Journal of Photochemistry and Photobiology A: Chemistry 148 (2002) 177-182. https://doi.org/10.1016/S1010-6030(02)00040-0

[94] D.L. Hoang, H. Lieske, Temperature-programmed reduction study of chromium oxide supported on zirconia and lanthana-zirconia, Thermochimica Acta 345 (2000) 93-99. https://doi.org/10.1016/S0040-6031(99)00385-8

[95] Z. Xie, Y. Ren, J. Li, Z. Zhao, X. Fan, B. Liu, W. Song, L. Kong, X. Xiao, J. Liu, G. Jiang, Facile in situ synthesis of highly dispersed chromium oxide incorporated into mesoporous ZrO2 for the dehydrogenation of propane with CO2, J Catal 372 (2019) 206–216. https://doi.org/10.1016/j.jcat.2019.02.026.

[96] Y. Yuan, Z. Zhao, R.F. Lobo, B. Xu, Site Diversity and Mechanism of Metal-Exchanged Zeolite Catalyzed Non-Oxidative Propane Dehydrogenation, Advanced Science 10 (2023). https://doi.org/10.1002/advs.202207756.

[97] I. Suzuki, Y. Kaneko, Dehydrogenation of Propane over Chromia-Alumina-Potassium Oxide Catalyst, J Catal 47 (1977) 239-248. https://doi.org/10.1016/0021-9517(77)90171-3

[98] C.A. Carrero, R. Schloegl, I.E. Wachs, R. Schomaecker, Critical literature review of the kinetics for the oxidative dehydrogenation of propane over well-defined supported vanadium oxide catalysts, ACS Catal 4 (2014) 3357–3380. https://doi.org/10.1021/cs5003417.

[99] Otroshchenko, T., Jiang, G., Kondratenko, V. A., Rodemerck, U., & Kondratenko, E. V. (2021). Current status and perspectives in oxidative, non-oxidative and CO 2-mediated dehydrogenation of propane and isobutane over metal oxide catalysts. *Chemical Society Reviews*, *50*(1), 473-527. 10.1039/D0CS01140A

[100] Han, S., Zhao, Y., Otroshchenko, T., Zhang, Y., Zhao, D., Lund, H., ... & Kondratenko, E. V. (2019). Unraveling the Origins of the Synergy Effect between ZrO2 and CrO x in Supported CrZrO x for Propene Formation in Nonoxidative Propane Dehydrogenation. *ACS catalysis*, *10*(2), 1575-1590. https://pubs.acs.org/doi/10.1021/acscatal.9b05063.

[101] Shivaji, Thapliyal, and Deo Goutam. "Propane dehydrogenation over alumina supported chromia catalysts." Bulletin of the Catalysis society of India 2 (2003): 29-33.

[102] M.A. Botavina, C. Evangelisti, Y.A. Agafonov, N.A. Gaidai, N. Panziera, A.L. Lapidus, G. Martra, CrOx/SiO2 catalysts prepared by metal vapour synthesis: Physical-chemical characterisation and functional testing in oxidative dehydrogenation of propane,

Chemical Engineering Journal 166 (2011) 1132–1138. https://doi.org/10.1016/j.cej.2010.11.070.

[103] J. Baek, H.J. Yun, D. Yun, Y. Choi, J. Yi, Preparation of highly dispersed chromium oxide catalysts supported on mesoporous silica for the oxidative dehydrogenation of propane using CO 2: Insight into the nature of catalytically active chromium sites, ACS Catal 2 (2012) 1893–1903. https://doi.org/10.1021/cs300198u.

[104] Michorczyk, Piotr, Piotr Pietrzyk, and Jan Ogonowski. "Preparation and characterization of SBA-1–supported chromium oxide catalysts for CO2 assisted dehydrogenation of propane." *Microporous and Mesoporous Materials* 161 (2012): 56-66. https://doi.org/10.1016/j.micromeso.2012.05.011

[105] Michorczyk, P., Ogonowski, J., & Niemczyk, M. (2010). Investigation of catalytic activity of CrSBA-1 materials obtained by direct method in the dehydrogenation of propane with CO2. *Applied Catalysis A: General*, *374*(1-2), 142-149. https://doi.org/10.1016/j.apcata.2009.11.040

[106] A. Węgrzyniak, S. Jarczewski, A. Węgrzynowicz, B. Michorczyk, P. Kuśtrowski, P. Michorczyk, Nanomaterials 7 (2017).

[107] Ghazimoradi, M., Najafi, A. M., Karami, H., Song, W., Liu, J., & Soltanali, S. (2025). Synergistic effects of cerium and zirconium as promoters on the performance of Cr/η-Al2O3 catalysts for propane dehydrogenation. *Fuel*, *394*, 135148. https://doi.org/10.1016/j.fuel.2025.135148

[108] S. Han, Y. Zhao, T. Otroshchenko, Y. Zhang, D. Zhao, H. Lund, T.H. Vuong, J. Rabeah, U. Bentrup, V.A. Kondratenko, U. Rodemerck, D. Linke, M. Gao, H. Jiao, G. Jiang, E. V. Kondratenko, "Unraveling the Origins of the Synergy Effect between ZrO2 and CrO x in Supported CrZrO x for Propene Formation in Nonoxidative Propane Dehydrogenation." *ACS catalysis* 10.2 (2019): 1575-1590. https://pubs.acs.org/doi/10.1021/acscatal.9b05063.

[109] S. Han, T. Otroshchenko, D. Zhao, H. Lund, U. Rodemerck, D. Linke, M. Gao, G. Jiang, E. V. Kondratenko, Catalytic non-oxidative propane dehydrogenation over promoted Cr-Zr-Ox: Effect of promoter on propene selectivity and stability." *Catalysis Communications* 138 (2020): 105956. https://doi.org/10.1016/j.catcom.2020.105956

[110] A. Węgrzyniak, S. Jarczewski, A. Wach, E. Hędrzak, P. Kuśtrowski, P. Michorczyk, "Catalytic behaviour of chromium oxide supported on CMK-3 carbon replica in the dehydrogenation propane to propene." *Applied Catalysis A: General* 508 (2015): 1-9. https://doi.org/10.1016/j.apcata.2015.10.002

[111] P.P. Li, W.Z. Lang, K. Xia, L. Luan, X. Yan, Y.J. Guo, "The promotion effects of Ni on the properties of Cr/Al catalysts for propane dehydrogenation reaction." *Applied Catalysis A: General* 522 (2016): 172-179. https://doi.org/10.1016/j.apcata.2016.05.007

[112] M.G. Cutrufello, S. De Rossi, I. Ferino, R. Monaci, E. Rombi, V. Solinas, "Preparation, characterisation and activity of chromia–zirconia catalysts for propane dehydrogenation." *Thermochimica acta* 434.1-2 (2005): 62-68. https://doi.org/10.1016/j.tca.2005.01.017

Declaration of interests

☒ The authors declare that they have no known competing financial interests or personal relationships that could have appeared to influence the work reported in this paper.

☐ The authors declare the following financial interests/personal relationships which may be considered as potential competing interests:

Graphical abstract

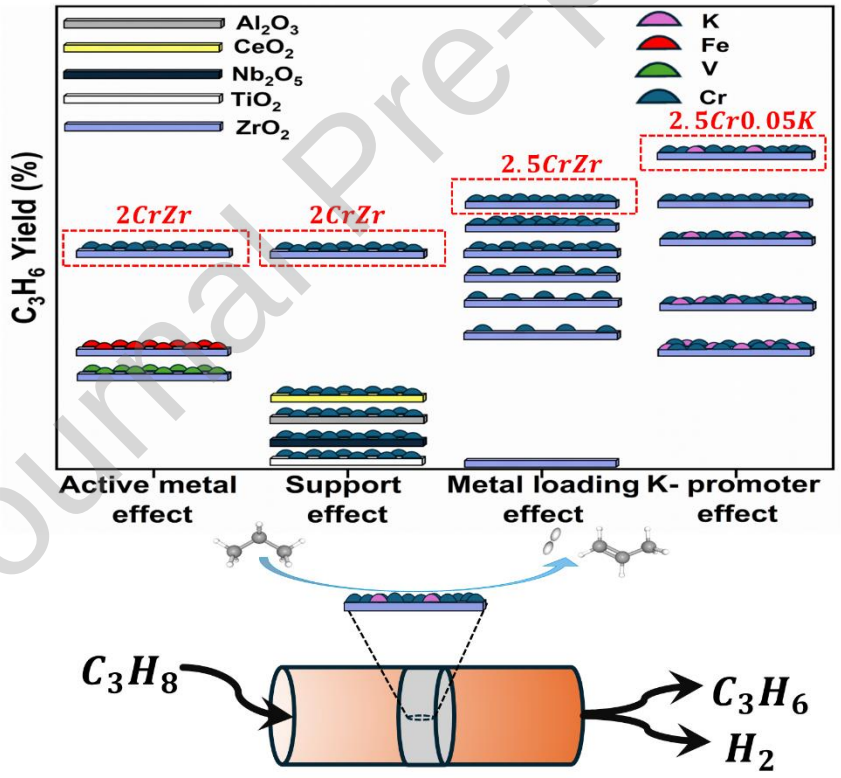

Highlights

- Chromium oxide supported ZrO_2, CrZr, is more active for DDP than V and Fe at 550°C
- CrZr is also more active that Al_2O_3, CeO_2, Nb_2O_5, TiO_2 supported catalyst for DDP
- 2.5% Cr loading, 2.5CrZr, possesses near-monolayer coverage and is the most active
- Limited amount of K, K/Cr = 0.05, on 2.5CrZr enhances DDP activity and selectivity
- ~30% conversion and ~27% C_3H_6 yield are achieved at 550°C and 37.33 $g_{cat}.h/mol$